ACTIVATION-RATE MEASUREMENTS IN THE ZPR-3 MOCKUP CRITICAL EXPERIMENTS

Part I. Measurements of Foil-activation Rates and Fission Yields in Assembly 60 of ZPR-3—Mockup of EBR-II with a Uranium Blanket

N. D. Dudey, R. R. Heinrich, R. J. Popek,
R. P. Larsen, and R. D. Oldham

U of C-AUA-USAEC

ARGONNE NATIONAL LABORATORY, ARGONNE, ILLINOIS

The facilities of Argonne National Laboratory are owned by the United States Government. Under the terms of a contract (W-31-109-Eng-38) between the U. S. Atomic Energy Commission, Argonne Universities Association and The University of Chicago, the University employs the staff and operates the Laboratory in accordance with policies and programs formulated, approved and reviewed by the Association.

MEMBERS OF ARGONNE UNIVERSITIES ASSOCIATION

The University of Arizona	Kansas State University	The Ohio State University
Carnegie-Mellon University	The University of Kansas	Ohio University
Case Western Reserve University	Loyola University	The Pennsylvania State University
The University of Chicago	Marquette University	Purdue University
University of Cincinnati	Michigan State University	Saint Louis University
Illinois Institute of Technology	The University of Michigan	Southern Illinois University
University of Illinois	University of Minnesota	The University of Texas at Austin
Indiana University	University of Missouri	Washington University
Iowa State University	Northwestern University	Wayne State University
The University of Iowa	University of Notre Dame	The University of Wisconsin

Printed in the United States of America
Available from
National Technical Information Service
U.S. Department of Commerce
5285 Port Royal Road
Springfield, Virginia 22151
Price: Printed Copy $3.00; Microfiche $0.95

ANL-7781
Reactor Technology

ARGONNE NATIONAL LABORATORY
9700 South Cass Avenue
Argonne, Illinois 60439

ACTIVATION-RATE MEASUREMENTS IN THE ZPR-3 MOCKUP CRITICAL EXPERIMENTS

Part I. Measurements of Foil-activation Rates and Fission Yields in Assembly 60 of ZPR-3—Mockup of EBR-II with a Uranium Blanket

by

N. D. Dudey, R. R. Heinrich, R. J. Popek,
R. P. Larsen, and R. D. Oldham

Chemical Engineering Division

April 1971

TABLE OF CONTENTS

LIST OF FIGURES

LIST OF FIGURES (Continued)

LIST OF FIGURES (Continued)

LIST OF TABLES

LIST OF TABLES (Continued)

ACTIVATION-RATE MEASUREMENTS IN THE ZPR-3 MOCKUP CRITICAL EXPERIMENTS

Part I. Measurements of Foil-activation Rates and Fission Yields in Assembly 60 of ZPR-3—Mockup of EBR-II with a Uranium Blanket

by

N. D. Dudey, R. R. Heinrich, R. J. Popek,
R. P. Larsen, and R. D. Oldham

ABSTRACT

This report is the first in a series that will discuss activation-rate measurements conducted in the ZPR-3 critical facility in mockup experiments designed to simulate various configurations of EBR-II. The primary objective of the reports is to describe these measurements and to present the results in a usable fashion.

This report represents a complete description of the activation-rate measurements conducted in Assembly 60 of ZPR-3. The study consisted of two experiments designed for different purposes. The first experiment was designed for dosimetry purposes to provide data necessary for characterizing the irradiation environment by means of activation-rate measurements. The second experiment was designed to provide data from which fast-neutron fission yields of various fission products could be established. Both experiments involved irradiations of foils near the center of the reactor core, near the core-blanket interface, and within the radial blanket. The reaction-rate data are presented, intercompared, and also compared with the results from a third activation-rate experiment conducted by an independent group.

I. INTRODUCTION

The Experimental Breeder Reactor-II (EBR-II) was originally designed and built to demonstrate the feasibility of operating sodium-cooled fast reactors. This objective was accomplished during the early operation of the reactor, and the reactor has now become an experimental irradiation facility for testing fast-reactor fuels and materials. Full utilization of EBR-II as a test reactor requires that its irradiation environment, namely, neutron flux, neutron spectrum, temperature, etc., be accurately characterized. The accuracy with which these conditions are known directly influences the success with which material irradiation-effects studies, fuel evaluation studies, and reactor design and safety experiments can be conducted within a test reactor.

A considerable amount of information concerning the irradiation environment of EBR-II has been obtained by measurements made within the reactor[1-5]. However, most of these measurements were made with the intent of characterizing the irradiation conditions for a specific experiment. The only comprehensive effort to map the neutron flux throughout the core of EBR-II was conducted in Runs 31E and 31F[1-3]. The studies in Runs 31E and 31F resulted primarily in clarifying the current capability for characterizing the irradiation environment of any fast test reactor (FTR). Dudey et al[1] and McElroy et al[2] have discussed this subject in detail. The outstanding problems associated with characterizing the irradiation environment of any FTR are as follows: (1) More accurate data on differential cross sections and fast-neutron fission yields must be obtained to interpret the foil

activation rate data. (2) A systematic comparison must be made of experimental activation-rate data with theoretically calculated activation rates so that confidence can be established in the calculational capability, basic nuclear data can be evaluated, and the causes and effects of spectral perturbations within the reactor can be understood more fully. (3) The observation of an apparent spectral shift in EBR-II as a function of reactor-power level must be understood. (4) The accuracy of each of the four methods available for flux characterization (foil activation, reactor-physics calculations, heat balance, and burnup) must be established and consistency among these methods obtained.

To this end, a comprehensive program to study the irradiation environment of EBR-II has been initiated. The program will also provide experimental information for evaluating both the effects of changes in EBR-II and designs of future FTRs upon their utility as test reactors. The program involves a series of measurements in the ZPR-3 critical facility in mockup experiments designed to simulate various configurations of EBR-II; these will be followed by a detailed flux-mapping study to be conducted in EBR-II.

This series of reports will describe part of the foil-activation-rate experiments conducted in the ZPR-3 mockup program. This report will discuss the activation rate measurements conducted in Assembly 60 of ZPR-3, in which the critical facility was mocked-up to simulate a homogeneous EBR-II core with a uranium blanket. Subsequent reports will discuss activation-rate data obtained in assemblies mocked-up to simulate different configurations of EBR-II.

Critical facility mockup experiments are particularly valuable because they are conducted at much lower power than the normal operating power of EBR-II. The low power environment permits the use of such instruments as proton-recoil counters for measurement of the neutron spectrum, fission counters for measurement of relative fission rates as a function of position, and thermoluminescent dosimeters for measurement of gamma heating; moreover, characterization of the irradiation environment by foil-activation rate measurements is also possible. By introducing various consistencies and symmetries within the composition of the mockup assemblies, more reliable theoretical calculations of the reactor are possible. This, in turn, enables a more complete and meaningful comparison of theory and experiment than is possible in EBR-II.

The objectives of the activation-rate measurements made in the mockup irradiations are as follows:

(1) To provide experimental activation-rate data from the low power mockup assemblies for nuclear reactions which will be measured at both low and high power in EBR-II. These data will enable a direct experimental comparison to be made of the irradiation environment in the mockup with the environment in the full scale reactor - EBR-II. In effect, these data will be a direct experimental demonstration of the degree with which a given mockup assembly simulates EBR-II.

(2) To provide measured nuclear reaction rates which may be compared with reaction rates derived from reactor physics calculations.

Examination of the heterogeneity effects within a drawer of the critical assembly is of particular interest. Essentially, the reaction-rate data obtained in the mockup assemblies will serve as bench-mark data with which to evaluate improvements in the calculational capability of fast-reactor physics codes.

(3) To evaluate the accuracies with which dosimetry data, namely, flux and neutron spectral information, can be deduced from activation-rate data.

(4) To measure accurately the ^{235}U, ^{238}U, and ^{239}Pu fission yields of a number of gamma-active fission products in EBR-II neutron spectra. The mockup irradiations provide a unique opportunity to carry out highly accurate fission-yield determinations - determinations which could not be carried out in EBR-II. These absolute fission yields are essential for burnup and dosimetry measurements in EBR-II as well as all future FTRs.

II. DESCRIPTION OF IRRADIATIONS IN ASSEMBLY 60

Assembly 60 of ZPR-3 was designed to simulate a 91-subassembly version of EBR-II. The core composition of this assembly represented a homogenized EBR-II loading except that the plutonium subassemblies of EBR-II were represented by ^{235}U in the assembly. The ^{235}U concentration differed slightly from that of EBR-II to minimize changes in the core for succeeding mockup assemblies. The Assembly-60 core-radial blanket boundary approached the hexagonal configuration of EBR-II. The radial blanket was similar in composition to EBR-II, as were the top and bottom axial reflectors; namely, each were asymmetric and consisted of a sodium-rich gap and a steel-rich reflector.

The ZPR-3 critical facility consists of honeycomb matrixes mounted on two cylindrical tables or halves, one of which is movable. A view of the honeycomb matrix pattern, as seen from the center looking at Half 1, is shown in Fig. 1. The matrixes are loaded with 2-in. by 2-in. drawers filled with plates containing the reactor materials. Figure 2 shows a front view of the plates for the core and blanket regions in the Assembly 60 configuration. A horizontal section of Assembly 60 is presented in Fig. 3, in which the several zones of the reactor are shown. The compositions of each of the zones are given in Table I. A more complete description of Assembly 60 is given in Ref. 6.

The foil-activation irradiations in Assembly 60 consisted of four distinct but complementary experiments. Each experiment consisted of various foil sets irradiated at the positions within the assembly shown in Fig. 1 and designated as D, Y, A, NS, and F. The dosimetry packets located in the D positions (near the core center, near the core-blanket interface, and in the blanket region) were identical for all three positions. These packets contained 1.97-in.-square metal foils of nickel, gold, uranium-235, and uranium-238. The foils and their corresponding thicknesses and typical weights are listed in Table II. The isotopic composition of the ^{235}U and ^{238}U is given in Table III. The uranium foils were individually wrapped in commercial aluminum foil (0.0005 in. thick) to contain any recoil fission fragments and to minimize cross contamination between foils. The individual

FIG. 1. Matrix Pattern and Foil-Packet Locations in the Assembly 60 Loading of ZPR-3 (Vertical Cross Section of Half No. 1)

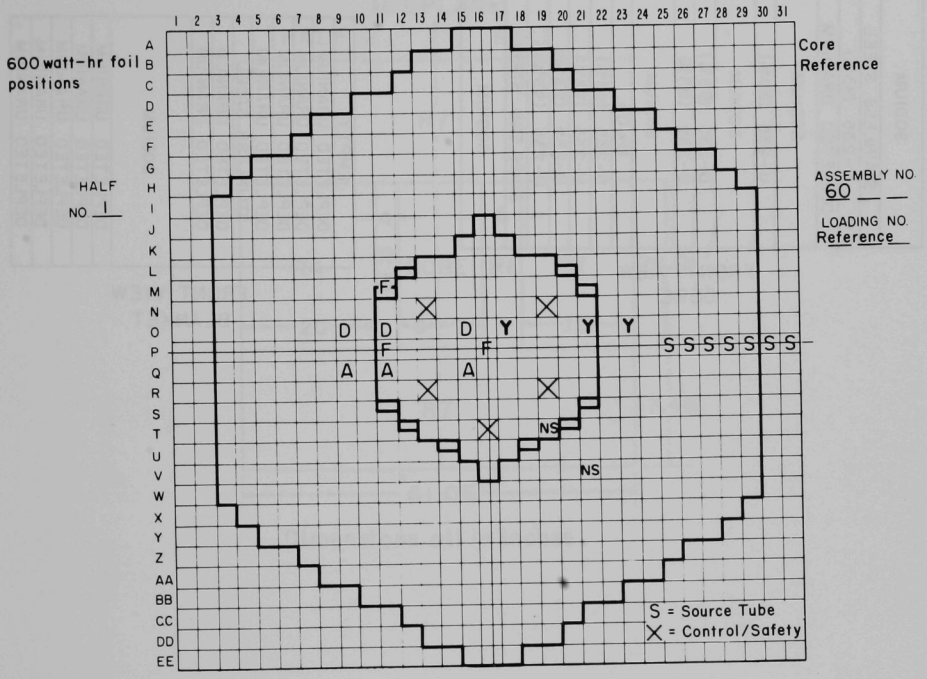

FIG. 2. Plate Configurations and Composition of the Core and Blanket Drawers of Assembly 60

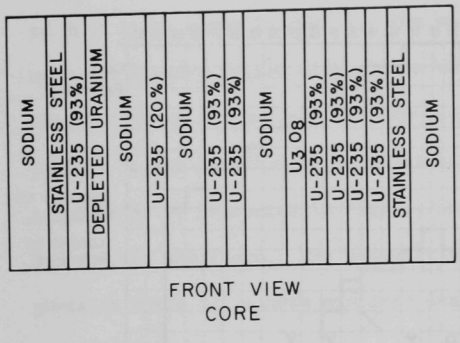

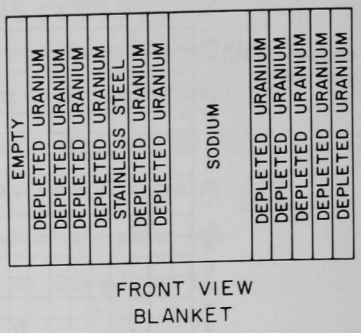

FIG. 3. Horizontal Cross Section of Assembly 60

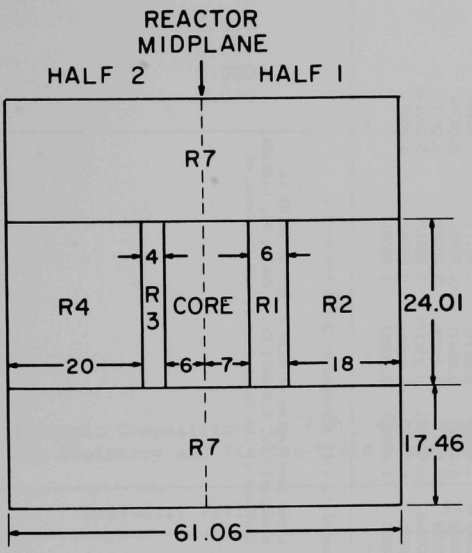

TABLE I: Composition of the Zones of Assembly 60

Element	Core: Half 1	Core: Half 2	Core[a] Average	Control and Safety Rods[a]	(R1) Upper Gap	(R2) Upper Reflector[b]	(R3) Lower Gap	(R4) Lower Reflector[b]	(R7) Radial Blanket: Half 1[b]	(R7) Radial Blanket: Half 2[b]
U-235	0.005578	0.005613	0.005594	0.005594	-	-	-	-	0.000055	0.000054
U-238	0.004571	0.004568	0.004570	0.004570	-	-	-	-	0.026505	0.026548
Na	0.01017	0.01052	0.01033	0.01033	0.01480	0.01029	0.01199	0.00898	0.00457	0.00455
Fe	0.01323	0.01353	0.01337	0.01462	0.01844	0.02802	0.02332	0.03175	0.00964	0.00963
Cr	0.00340	0.00347	0.00343	0.00364	0.00480	0.00762	0.00622	0.00881	0.00254	0.00253
Ni	0.00148	0.00151	0.00149	0.00159	0.00209	0.00331	0.00271	0.00382	0.00111	0.00110
Mn	0.000171	0.000174	0.000172	0.000152	0.000260	0.000501	0.000379	0.000626	0.000146	0.000145
Si	0.00013	0.00013	0.00013	0.00017	0.00015	0.00012	0.00014	0.00007	0.00007	0.00007
Mo	-	-	-	-	0.00001	0.00003	0.00002	0.00004	-	-
O	0.002137	0.002132	0.002135	0.002135	-	-	-	-	-	-

[a]This represents a core average weighed in terms of the geometric arrangement, with a weight of 0.538 for Half 1 and of 0.462 for Half 2.

[b]Spring gap (0.66 cm wide) is located 21.03 in. from interface in Half 1 and core region of Half 2, and is 15.03 in. from interface in radial blanket of Half 2. Its composition is (10^{24} atoms/cc): Fe, 0.01685; Cr, 0.00419; Ni, 0.00184; Mn, 0.000175; and Si, 0.00020. This composition includes the spring, the back of the front drawer, and the front of the back drawer.

TABLE II. Weights and Thicknesses of 2-in. by 2-in. Foils in Dosimetry Packets

Monitor	Thickness (in.)	Weight (g)
Nickel	0.010	5.5
Uranium-235	0.006	7.1
Gold	0.0002	0.2
Uranium-238	0.010	11.0

TABLE III. Isotopic Compositions of ^{238}U, ^{235}U, and ^{239}Pu Foils in Dosimetry and Fission-Yield Packets

Material	Dosimetry Foils	Fission-Yield Foils
^{238}U	99.78% ^{238}U 0.22% ^{235}U	99.78% ^{238}U 0.22% ^{235}U
^{235}U	93.10% ^{235}U 6.90% ^{238}U	93.12% ^{235}U 0.96% ^{234}U 0.32% ^{236}U 5.59% ^{238}U
^{239}Pu		94.61% ^{239}Pu 5.06% ^{240}Pu 0.31% ^{241}Pu 0.02% ^{242}Pu

foils were stacked in the order given in Table II and then wrapped together in the same type aluminum foil to constitute an individual packet of foils. The total weight of aluminum in each packet was about 1 g. The packets were identified for orientation in the assembly and for drawer position. An assembled packet is shown in Fig. 4. The packets were inserted into the assembly perpendicularly to the plates in the drawer and located about 1 in. from the physical mid-plane of the split-table assembly.

The objective of the Y-foil experiments was to determine the yields of gamma-active fission products produced from the fission of ^{239}Pu, ^{235}U, and ^{238}U in various neutron spectra. These foil packets, which were perpendicular to the fuel plates, were located in positions symmetric with the D packets (see Fig. 1). The holder used to contain the samples for irradiation in the Y experiment is shown in Fig. 5. One side of the irradiation holder contained mica fission-track recorders in contact with nanogram quantities of fissile material which had been electrodeposited as uniformly dispersed spots on platinum strips. The other side of the irradiation holder contained gram amounts of the fissile nuclides as metal foils. Figure 5 illustrates the physical orientation of the track recorders, the nanogram samples, and the gram foil samples of fissile material within the irradiation holder. A description of the methods used for preparation of the track recorders and deposition of nanogram amounts of fissile material onto the platinum plates is presented in Appendix A. The sample identification schemes of both the mica track recorders and the foil samples are

FIG. 4. Cut-Away Side View of Dosimetry Foil Packet

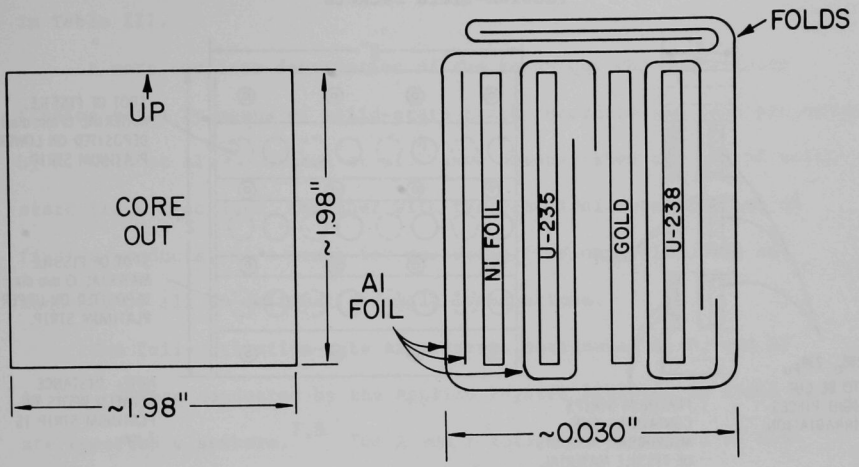

FIG. 5. Cut-Away Side and End View of Fission-Yield Packets

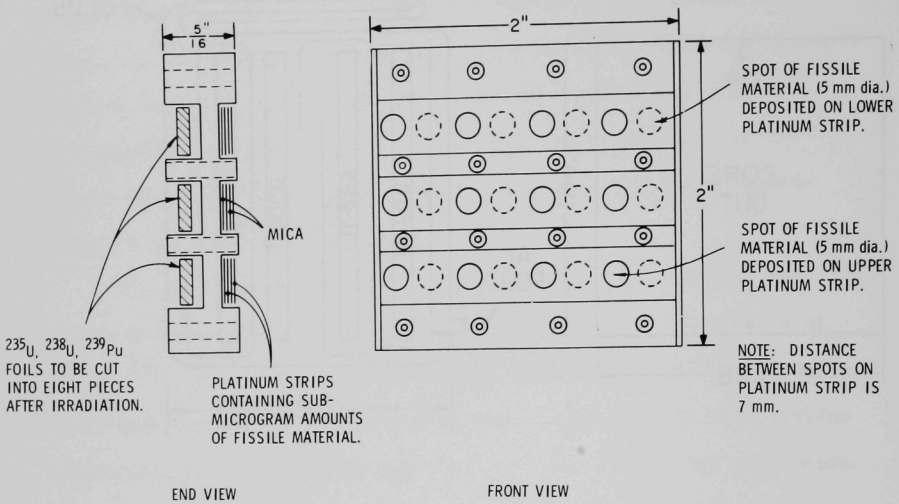

shown in Figs. 6, 7, and 8 for the core, interface, and blanket holders, respectively. The isotopic composition of the foil samples is given in Table III.

A more complete description of the technique for determining fission rates by means of solid-state track recorders has been presented by R. Gold et al.[10] Armani et al.[9] have demonstrated the use of solid-state track recorders, together with radiochemical determination of fission products, as a means for measuring fission yields with an accuracy of ±1% in critical assembly irradiations.

The foil-activation-rate experiments designated A, F, and NS in Fig. 1 were conducted by the Applied Physics Division in Idaho and are reported elsewhere.[7,8] The A and F foil sets consisted of 0.5-in.-dia by 0.005-in.-thick foils of ^{235}U, ^{238}U, aluminum, tungsten, gold, and indium. The A foils were positioned between selected plates in positions symmetric with the D foils. The A and D foil sets were designed to be complementary, with the D sets being perpendicular to and the A sets being parallel to the fuel plates. The F experiments were designed to examine spectral effects due to structural boundaries. The NS sets consisted of 19 individual foils contained in cubical containers (2 by 2 by 2 in.); the purpose of this experiment was to provide activation-rate data from which neutron spectral information might be deduced. For further information on the A, F, and NS foils see references 7 and 8.

All of the foil-activation-rate samples were irradiated simultaneously for a period of 61 min in ZPR-3. The irradiation

terminated at 1201 MST on February 26, 1970. The D and Y samples were received at Argonne-Illinois for analysis 19 hr after the end of the irradiation.

III. EXPERIMENTAL ANALYSIS OF THE IRRADIATED SAMPLES

A. Preparation of Samples for Counting

Upon receipt of the samples, the foil packets were opened and the 2-in. by 2-in. dosimetry (D) foils were then cut into smaller pieces for counting. The dimensions of the cut pieces and the identification scheme is shown in Fig. 9. The objective of this cutting scheme was to establish the heterogeneity effects due to the plate composition of the assembly drawers and to correlate this information with the A foil sets being measured by another group. The order in which the samples were cut was chosen to minimize any possible cross contamination.

The fission-yield (Y) samples were handled in a similar manner. The platinum plates and mica track recorders were first removed and stored for later analysis. Appendix B describes the procedures employed to determine the amounts of fissile material present on the platinum plates. The ^{238}U, ^{235}U, and ^{239}Pu foils were removed from the aluminum holders and the foils were cut into 1/4-in. sections according to the patterns presented in Fig. 6-8. Of these sections, those numbered 5CL-7, 5IL-7, 5BL-7, 8CL-7, 8IL-7, and 8BL-7 were reserved for radiochemical determinations of ^{99}Mo and ^{140}Ba. The remaining sections were mounted for gamma-counting.

FIG. 6. Sample-Identification Scheme for Fission-Yield Core Packet

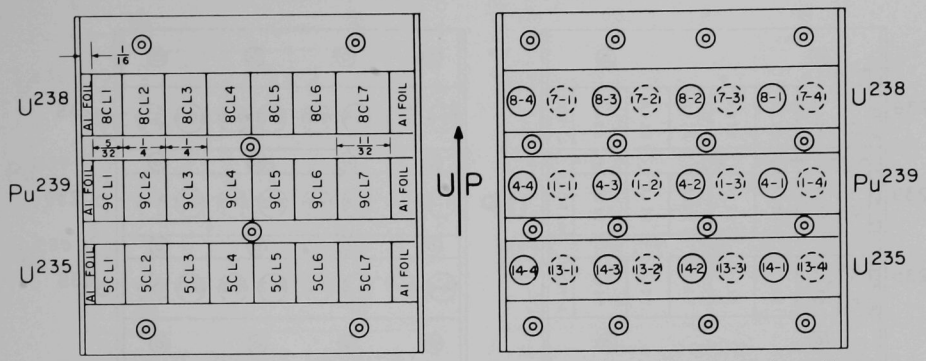

CORE

FIG. 7. Sample-Identification Scheme for Fission-Yield Interface Packet

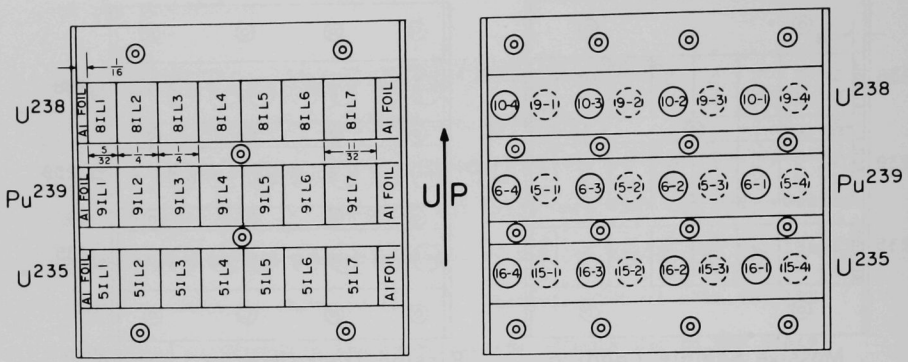

FIG. 8. Sample-Identification Scheme for Fission-Yield Blanket Packet

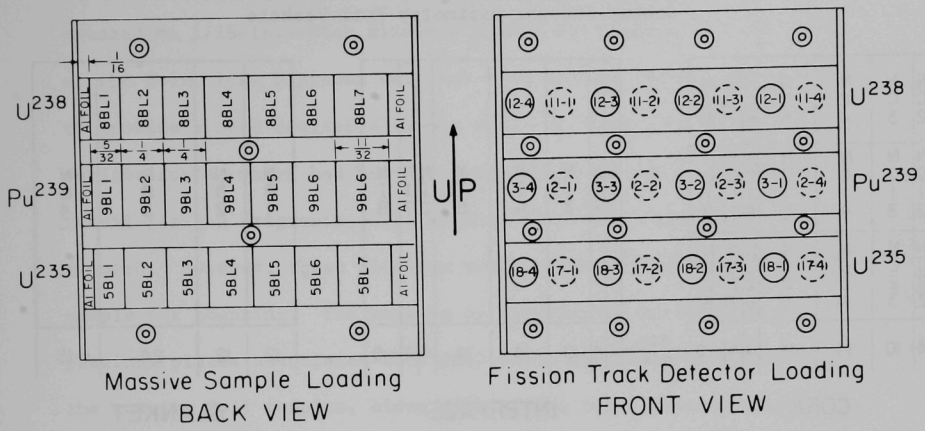

BLANKET

FIG. 9. Cutting Diagram and Sample-Identification Scheme for the Dosimetry Foil Packets

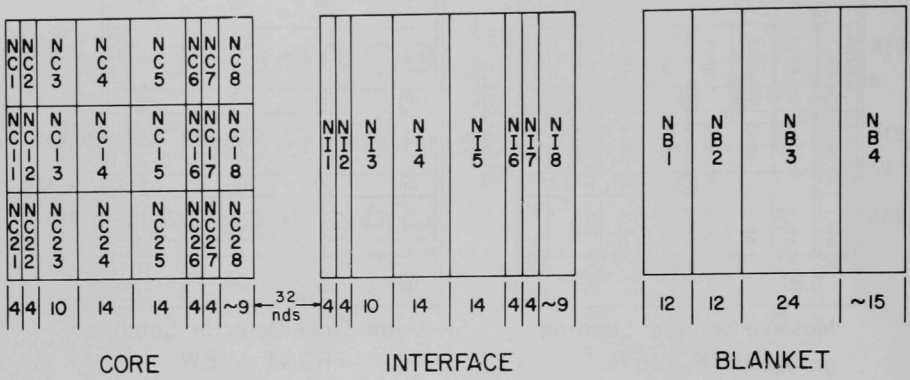

Subsequent to cutting, the Y and D foil sections were analyzed identically. The samples were individually weighed and mounted on 1/16-in.-thick aluminum plates for gamma-counting. Some of the 2-in. long D pieces were cut into smaller pieces and stacked to provide a more desirable sample shape for counting. The fission monitor foils, which had been wrapped with aluminum to catch any recoil fission fragments, were weighed after the aluminum had been removed. However, these aluminum covers were mounted alongside the sample for counting. The weights of fissionable material on the platinum plates associated with each track recorder and weights of the massive foil samples, along with sample identification numbers, are given in Tables IV, V, and VI for ^{239}Pu, ^{235}U, and ^{238}U, respectively. The weights and sample numbers for the dosimetry foils are given in Tables VII and VIII.

B. Gamma-Counting of Irradiated Samples

Counting of the samples was begun about 24 hr after the end of the irradiation. The uranium and plutonium samples from both the D and Y foil sets were assayed on lithium-drifted germanium [Ge(Li)] detector systems to measure the fission products. The fission-yield (Y) samples were gamma-counted with a 10-cm^3 planar-type Ge(Li) detector having a full width at half maximum resolution (FWHM) of about 2.2 keV for the 1.33-MeV line of ^{60}Co. This detector was coupled to a 4096-channel pulse-height analyzer equipped with a magnetic-tape readout system. The dosimetry samples were counted on two Ge(Li) detector systems with respective ^{60}Co resolutions (FWHM) of 3.4 and

TABLE IV. Weights of ^{239}Pu Samples in the Fission-Yield Packets

Foil Samples		Track Recorder Samples	
Sample No.	Weight (mg)	Sample No.	Weight (ng)
9BL-1	268	2-4	49.3
9BL-2	601	3-1	45.2
9BL-3	532	2-3	35.3
9BL-4	573	3-2	56.3
9BL-5	520	2-2	59.2
9BL-6	574	3-3	50.8
9BL-7	412	2-1	51.4
9BL-7	412	3-4	45.3
9IL-1	309	5-4	56.7
9IL-2	487	6-1	59.7
9IL-3	574	5-3	55.2
9IL-4	598	6-2	43.2
9IL-5	553	5-2	63.9
9IL-6	616	6-3	55.9
9IL-7	384	5-1	62.0
9IL-7	384	6-4	47.0
9CL-1	401	1-4	10.18
9CL-2	637	4-1	3.86
9CL-3	-	1-3	7.51
9CL-4	619	4-2	9.04
9CL-5	524	1-2	7.32
9CL-6	482	4-3	9.42
9CL-7	321	1-1	9.04
9CL-7	321	4-4	13.68

TABLE V. Weights of ^{235}U Samples in the Fission-Yield Packets

Foil Samples		Track Recorder Samples	
Sample No.	Weight (mg)	Sample No.	Weight (ng)
5BL-1	356.4	17-4	117.6
5BL-2	423.1	18-1	118.0
5BL-3	543.2	17-3	102.6
5BL-4	361.0	18-2	141.1
5BL-5	497.3	17-2	86.6
5BL-6	433.5	18-3	98.5
5BL-7	a	17-1	116.2
5BL-7	a	18-4	113.1
5IL-1	360.3	15-4	34.4
5IL-2	500.4	16-1	31.6
5IL-3	480.6	15-3	38.7
5IL-4	500.4	16-2	b
5IL-5	496.7	15-2	40.7
5IL-6	537.6	16-3	28.8
5IL-7	a	15-1	36.0
5IL-7	a	16-4	25.7
5CL-1	367.1	13-4	14.92
5CL-2	578.3	14-1	16.68
5CL-3	467.1	13-3	18.42
5CL-4	536.6	14-2	14.48
5CL-5	505.9	13-2	19.25
5CL-6	577.7	14-3	11.08
5CL-7	a	13-1	7.73
5CL-7	a	14-4	15.64

[a]Value not yet determined.

[b]Sample lost.

TABLE VI. Weights of ^{238}U Samples in Fission-Yield Packets

Foil Samples		Track Recorder Samples	
Sample No.	Weight (mg)	Sample No.	Weight (ng)
8BL-1	890.9	11-4	a
8BL-2	1041.4	12-1	a
8BL-3	1289.7	11-3	a
8BL-4	1150.3	12-2	a
8BL-5	923.2	11-2	a
8BL-6	1297.3	12-3	a
8BL-7	a	11-1	a
8BL-7	a	12-4	a
8IL-1	814.5	9-4	730
8IL-2	1216.1	10-1	1055
8IL-3	1236.7	9-3	818
8IL-4	1139.0	10-2	866
8IL-5	1124.5	9-2	1001
8IL-6	1077.6	10-3	1050
8IL-7	a	9-1	711
8IL-7	a	10-4	809
8CL-1	975.2	7-4	224
8CL-2	1003.7	8-1	240
8CL-3	1263.7	7-3	236
8CL-4	1050.3	8-2	235
8CL-5	1247.6	7-2	192.9
8CL-6	1198.2	8-3	226
8CL-7	a	7-1	204
8CL-7	a	8-4	241

[a]Value not yet determined.

TABLE VII. Weights of ^{235}U and ^{238}U Samples Cut from Dosimetry-Packet Foils

^{235}U Samples				^{238}U Samples			
Sample No.	Wt. (mg)	Sample No.	Wt. (mg)	Sample No.	Wt. (mg)	Sample No.	Wt. (mg)
5B-1	1391.7	5C-1	144.0	8B-1	2033.8	8C-1	202.0
-2	1374.5	-2	147.1	-2	2230.1	-2	227.2
-3	2762.0	-3	384.5	-3	4202.0	-3	581.3
-4	1552.1	-4	513.3	-4	2476.1	-4	844.3
5I-1	442.3	-5	522.8	8I-1	671.2	-5	802.4
-2	438.4	-6	149.9	-2	672.5	-6	227.0
-3	1168.4	-7	157.5	-3	1893.7	-7	232.5
-4	1574.3	-8	316.0	-4	2418.3	-8	619.4
-5	1591.5	-11	140.9	-5	2455.8	-11	200.6
-6	465.0	-12	152.4	-6	666.5	-12	243.9
-7	445.8	-13	395.1	-7	662.7	-13	644.1
-8	956.4	-14	521.0	-8	1587.0	-14	880.9
		-15	532.8			-15	905.0
		-16	152.9			-16	263.7
		-17	157.5			-17	280.5
		-18	332.5			-18	573.2
		-21	136.3			-21	194.6
		-22	145.9			-22	240.5
		-23	386.8			-23	642.1
		-24	527.7			-24	867.0
		-25	535.0			-25	891.0
		-26	145.8			-26	258.3
		-27	155.2			-27	278.6
		-28	329.0			-28	563.0

TABLE VIII. Weights of Gold and Nickel Samples Cut from Dosimetry-Packet Foils

Gold Samples				Nickel Samples			
Sample No.	Wt. (mg)	Sample No.	Wt. (mg)	Sample No.	Wt. (mg)	Sample No.	Wt. (mg)
GB-1	45.7	GC-1	4.2	NB-1	1096.2	NC-1	116.6
-2	44.1	-2	4.6	-2	1067.6	-2	121.3
-3	87.5	-3	12.1	-3	2121.3	-3	309.5
-4	57.0	-4	16.7	-4	1362.0	-4	416.3
GI-1	11.9	-5	16.8	NI-1	338.7	-5	420.9
-2	14.6	-6	4.9	-2	348.7	-6	118.9
-3	38.0	-7	5.0	-3	919.5	-7	125.0
-4	50.8	-8	11.4	-4	1224.1	-8	272.3
-5	51.2	-11	4.5	-5	1233.2	-11	115.1
-6	14.2	-12	4.2	-6	350.5	-12	113.3
-7	14.6	-13	11.4	-7	341.3	-13	302.4
-8	34.4	-14	15.7	-8	805.3	-14	399.2
		-15	15.3			-15	407.4
		-16	4.2			-16	114.6
		-17	4.7			-17	118.9
		-18	11.3			-18	265.5
		-21	4.0			-21	115.7
		-22	4.5			-22	119.9
		-23	11.9			-23	310.6
		-24	15.8			-24	414.3
		-25	16.1			-25	421.7
		-26	4.8			-26	115.9
		-27	4.7			-27	122.1
		-28	10.8			-28	273.7

2.7 keV. The poorer resolution detector was pulse-height-analyzed using a 1024-channel analyzer and the other utilized a 1600-channel analyzer. Data readout from these two analyzers was in the form of punched paper tape. Both the magnetic tape and punched paper tape readouts were compatible input forms for computer analysis of the pulse-height spectra.

The gold and nickel samples were counted on a 4 by 4-in. NaI(Tl) detector system. These samples were first checked on the high-resolution Ge(Li) detectors to assure that they were free from any gamma activities which might interfere. The NaI(Tl) detector was coupled to a 512-channel pulse-height analyzer equipped for typewriter readout of the data. These counting data were manually analyzed.

1. Detector Calibration

Calibration of the Ge(Li) detectors was accomplished in the following manner: System linearity and relative detector efficiency were determined for each detector from the known gamma-ray energies and branching ratios of ^{152}Eu. The relative efficiencies were converted to absolute values by normalizing to point-source mounts of ^{57}Co, ^{137}Cs, ^{134}Cs, ^{54}Mn, and ^{60}Co. Absolute standards for the calibration were obtained from the Amersham Radiochemical Center and the National Bureau of Standards. The NaI(Tl) detector was calibrated using the same standards.

2. Counting Procedures

The general counting philosophy was influenced by the large number of samples (198), the low levels of many of the fission-product activities, and the relatively massive amounts and sizes of

some of the samples. To satisfy these constraints, each nuclide was counted three times within the time period defined by three half-lives from the end of the irradiation. If the three counts did not agree to within ±5% (after correcting for decay) a fourth count was taken. The principal gamma-ray of each nuclide was counted for a sufficient length of time to provide a minimum error of 3% due to counting statistics.

The counting geometries were adjusted to provide a maximum count rate without exceeding 18% dead time within the analyzer. Many of the fission-product samples were counted through external absorbers to reduce the bremsstrahlung background and natural low-energy interferences which introduced considerable dead time into the analyzers. The analyzers were operated in the live-time mode and had previously been calibrated for counting error as a function of dead time. For these sample counting rates, the error due to dead-time corrections was less than 2%.

C. Data Reduction and Analysis

The magnitude and complexity of the counting data made it imperative that computation and analysis be executed with the aid of a computer. We have adapted the computer code for gamma-ray analysis, originally written by Gunnink et al.[11], for this purpose. A brief description of the modified code, BILE, is presented in Appendix C. BILE requires as input the multichannel-analyzer counting data, detector efficiency and linearity, and decay-scheme information. The code computes the number of atoms of each nuclide present at the end of the irradiation, a statistical analysis of the reliability of each result, and a plot of the spectrum. Table IX summarizes the

TABLE IX. Decay Scheme Data Used in the Analysis of Gamma-Ray Spectra

Nuclide	Half-Life (days)	Energy (keV)	Branching Ratio
^{143}Ce	1.375	293.0	0.46
^{131}I	8.050	364.5	0.82
^{103}Ru	40.000	497.0	0.88
^{97}Zr	0.7008	745.0	0.94
$^{97}Zr(Nb)$	0.050	658.2	0.99
$^{132}I(Te)$	3.250	667.5	0.98
$^{140}La(Ba)$	12.800	1597.0	0.96
^{95}Zr	65.000	757.3	0.55
$^{95}Zr(Nb)$	35.000	765.8	0.99
^{239}Np	2.350	277.9	0.15
^{198}Au	2.690	411.8	0.95
^{58}Co	71.300	810.0	0.99

pertinent decay-scheme data for nuclides which are reported. Figures 10 through 17 show some typical gamma-ray spectra obtained from ^{235}U, ^{238}U, and ^{239}Pu samples counted approximately 1 day, 20 days, and 70 days after the irradiation.

Several corrections not included in the BILE code must be applied to the BILE output before final analysis is complete. These corrections were made by another computer code and are individually discussed below.

1. Geometry Corrections

The efficiency calibrations of each of the Ge(Li) detectors, which are used by the BILE program, were determined by counting point-source standards. The samples counted in this experiment differed in two ways from point sources; namely, they had finite thicknesses and finite areas, both of which varied from sample to sample. Corrections for these factors had to be made individually for each sample.

The correction factors for the thickness of the samples were determined experimentally as follows: A point-source ^{137}Cs standard was counted directly on an aluminum plate identical to the plates on which the samples were mounted. This point source was then moved (by insertion of spacers) in increments of 10 mils toward the detector (above the aluminum plate) and counted in each position. From a plot of the percent change in count rate as a function of distance above the aluminum plate and from the thickness of each sample, the thickness

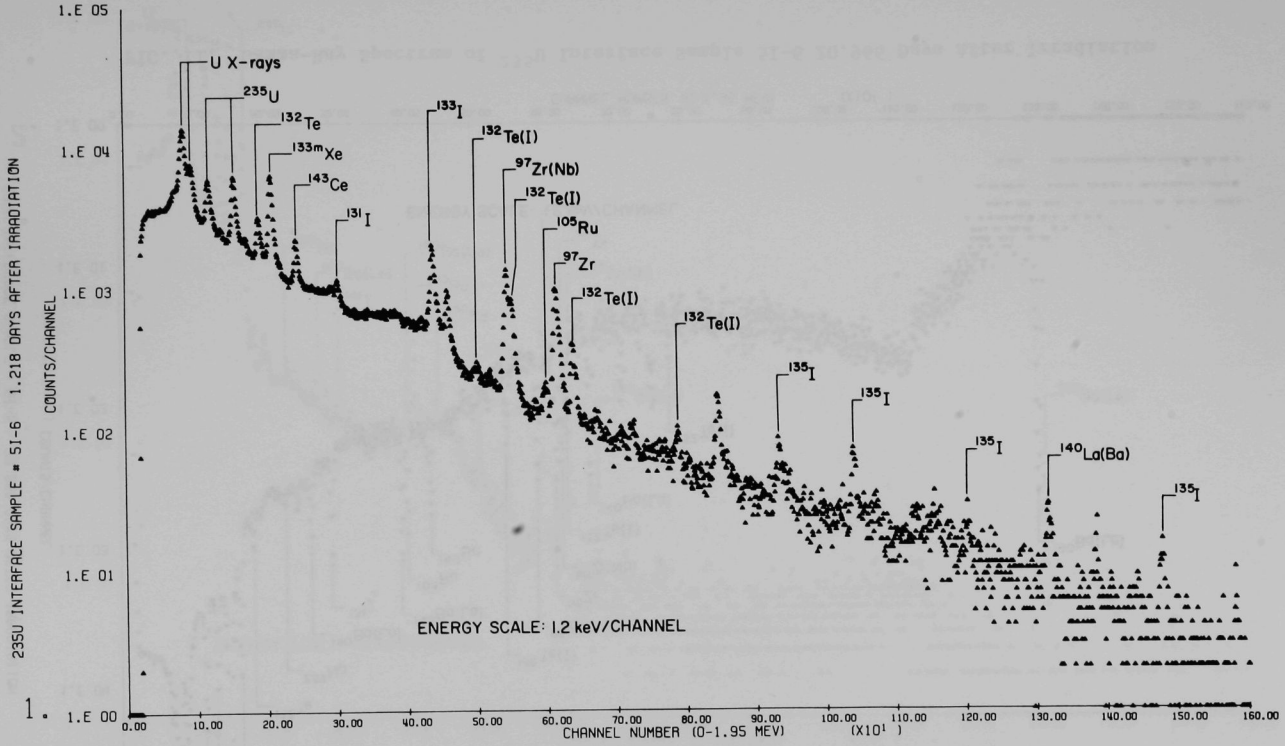

FIG. 10. Gamma-Ray Spectrum of ^{235}U Interface Sample 5I-6 1.218 Days After Irradiation

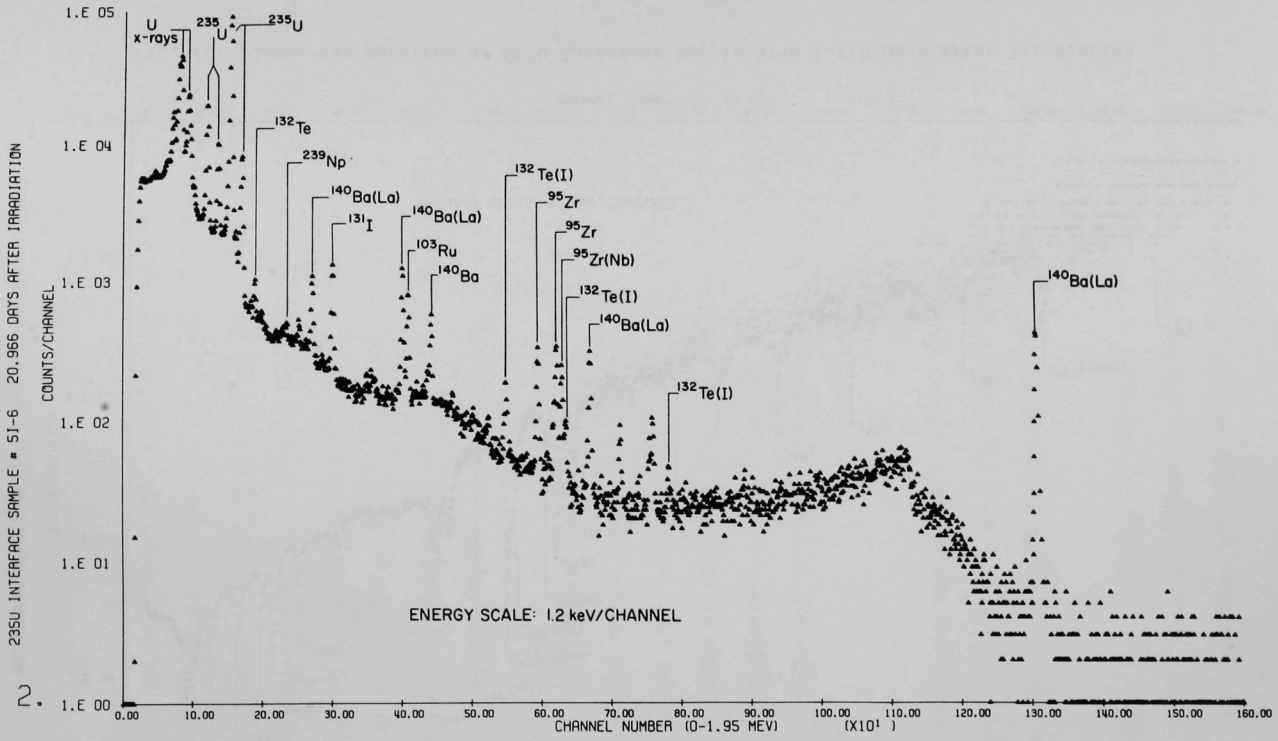

FIG. 11. Gamma-Ray Spectrum of ^{235}U Interface Sample 5I-6 20.966 Days After Irradiation

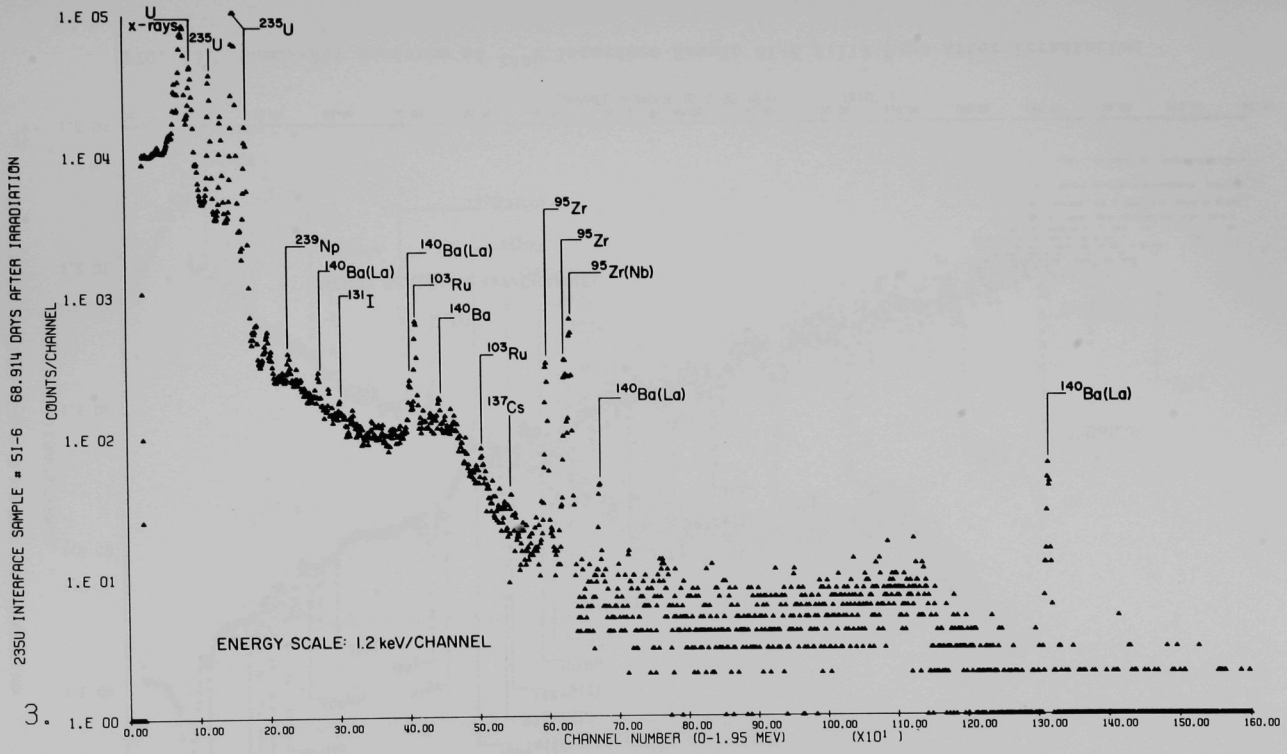

FIG. 12. Gamma-Ray Spectrum of ^{235}U Interface Sample 5I-6 68.914 Days After Irradiation

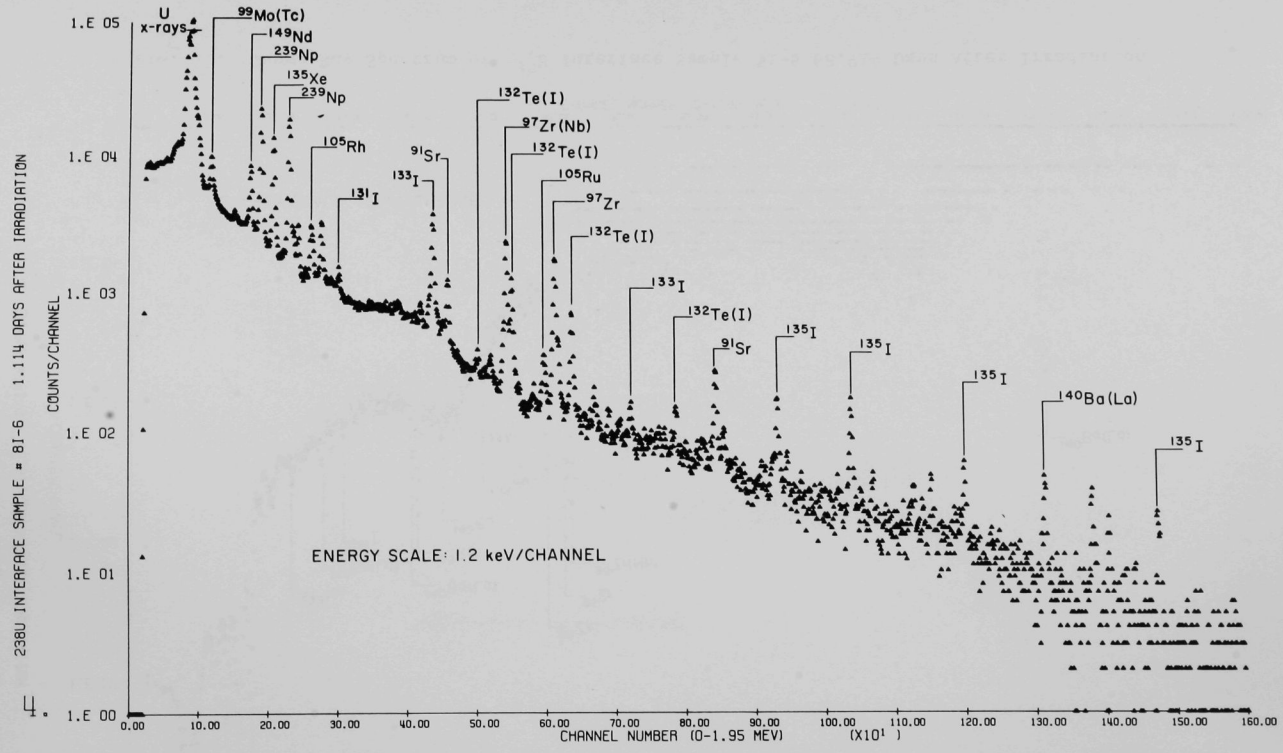

FIG. 13. Gamma-Ray Spectrum of ^{238}U Interface Sample 8I-6 1.114 Days After Irradiation

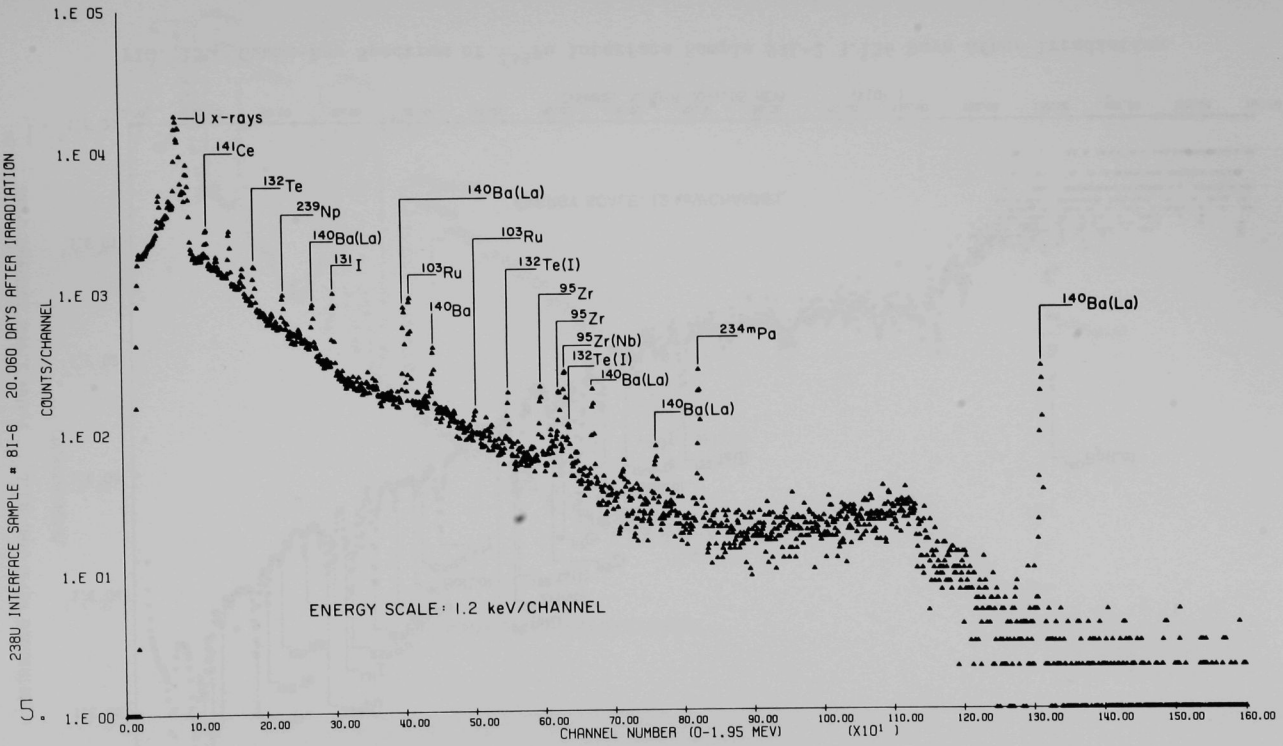

FIG. 14. Gamma-Ray Spectrum of ^{238}U Interface Sample 8I-6 20.060 Days After Irradiation

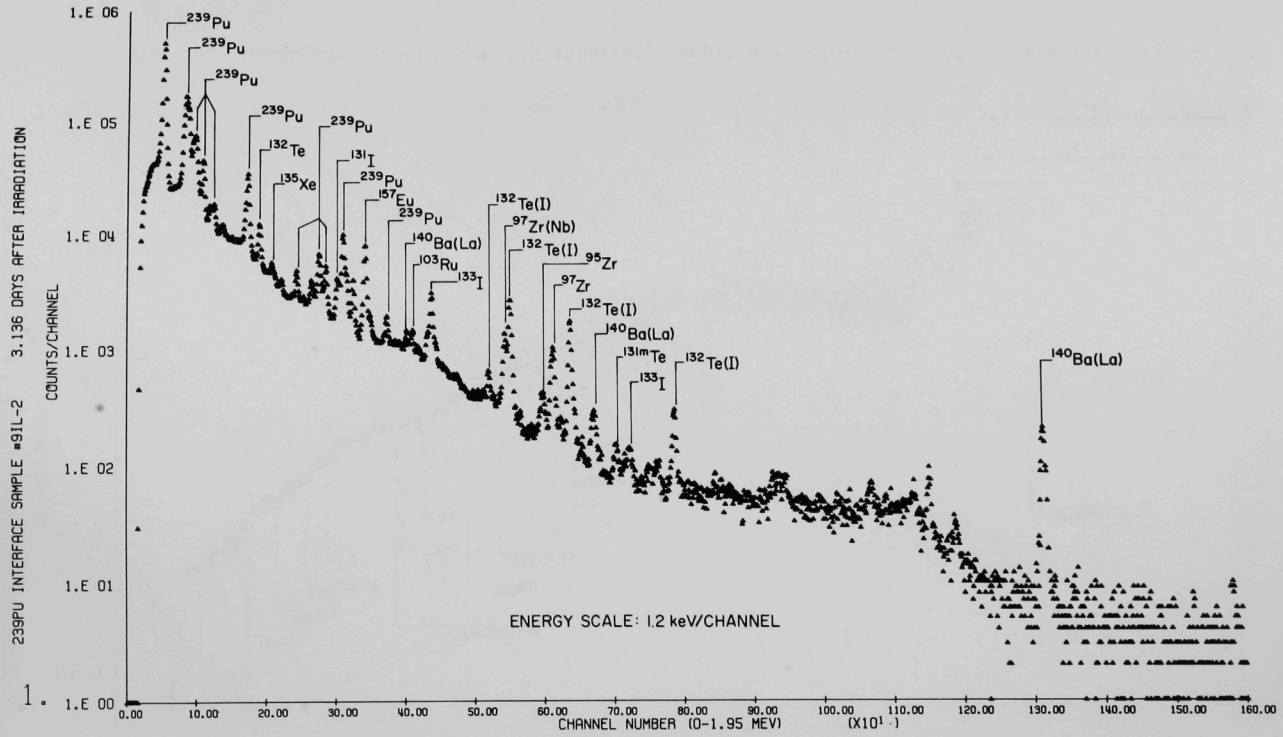

FIG. 15. Gamma-Ray Spectrum of ^{239}Pu Interface Sample 9IL-2 3.136 Days After Irradiation

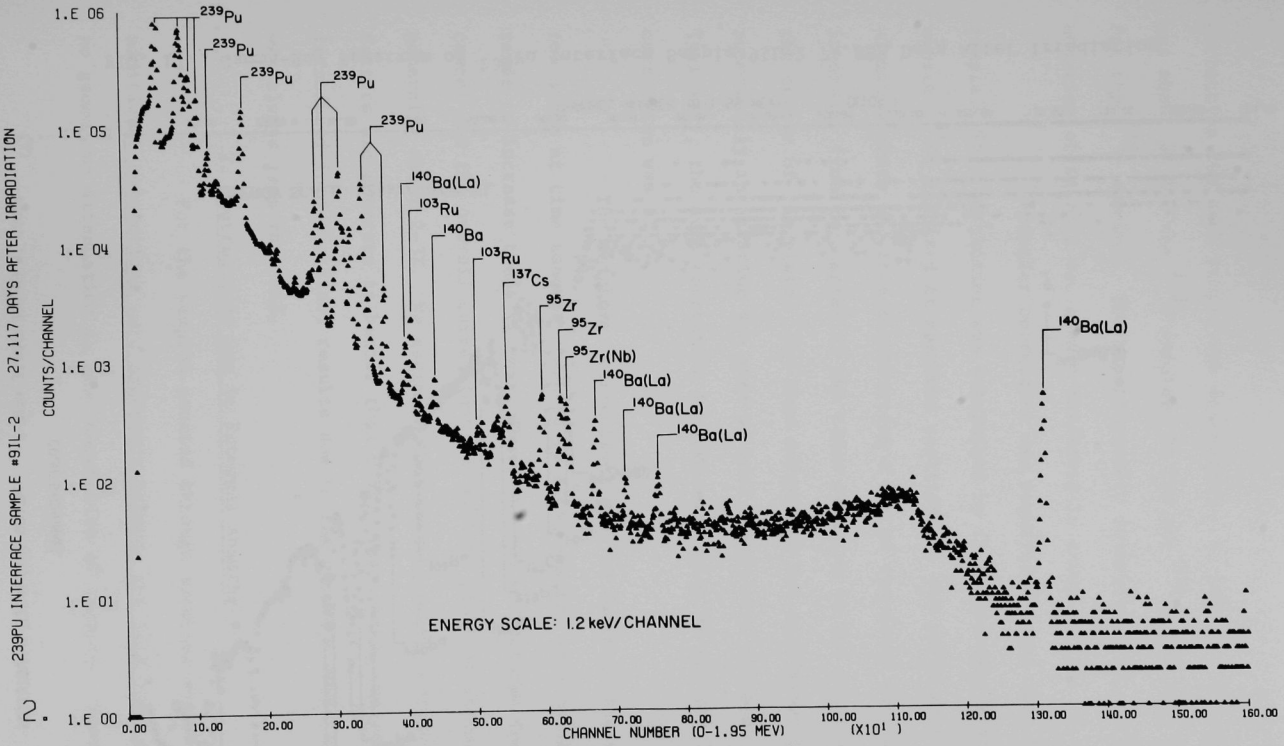

FIG. 16. Gamma-Ray Spectrum of ^{239}Pu Interface Sample 9IL-2 27.117 Days After Irradiation

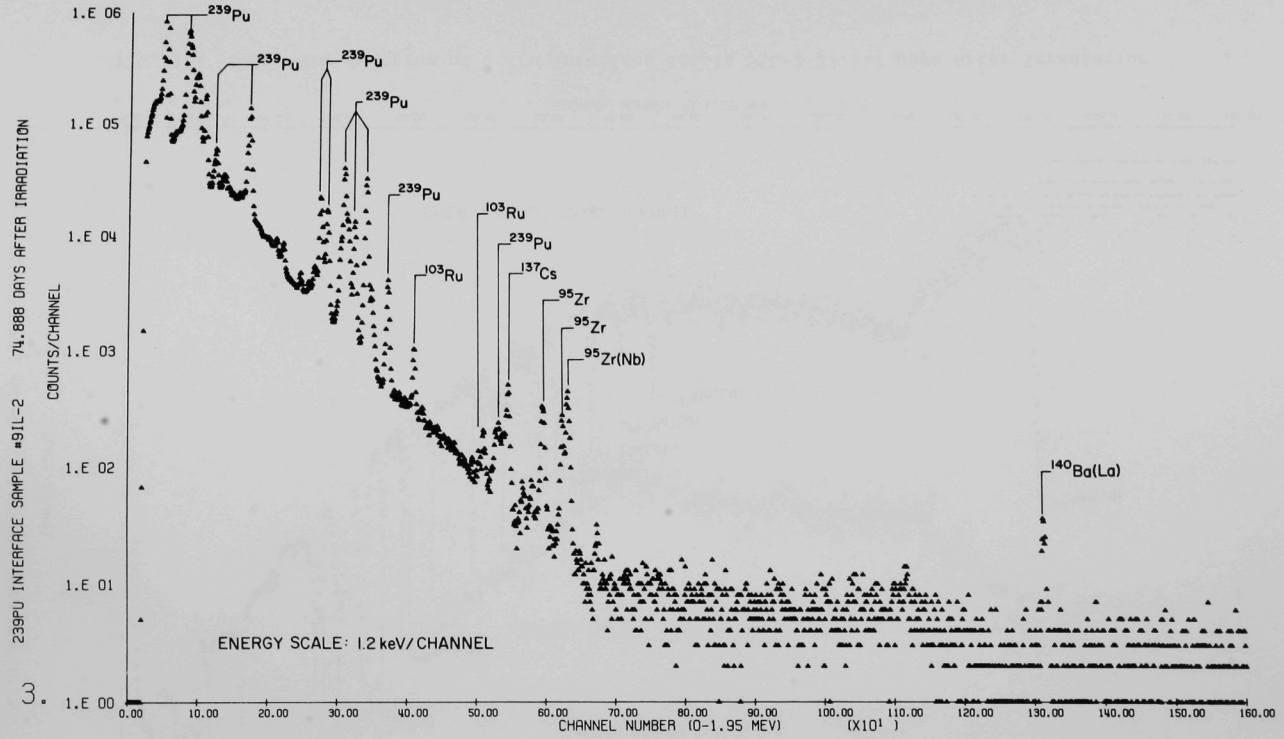

FIG. 17. Gamma-Ray Spectrum of ^{239}Pu Interface Sample 9IL-2 74.888 Days After Irradiation

correction for each sample was determined. In general, the correction was about 4% for the ^{235}U samples, 5% for the ^{239}Pu samples, and 6% for the ^{238}U samples. The experimentally determined plot of relative counting efficiency vs. sample thickness is shown in Fig. 18.

A similar correction was required for the area of each sample. This correction was determined by first counting a point-source ^{137}Cs standard at numerous positions on the surface of an aluminum plate and then constructing a map of the count rate at 1/8-in. intervals from the center of the plate relative to the count rate at the center of the plate. The area correction was determined by numerically integrating the area of each sample over the map. Typically, the area correction factors were about 3% and the largest correction was 5%.

The thickness corrections tend to decrease the values for atoms at time zero as computed by BILE, and the area correction tends to increase these values. Thus, the two corrections tend to cancel and the overall corrections due to both geometry factors were generally about 2-3%. We estimate that these geometry-correction factors are accurate to better than ±15%. The overall uncertainty introduced into the final results due to the geometry corrections was always less than ±1%.

2. Corrections Due to External Absorbers

For the samples counted through external absorbers, additional corrections were necessary because the BILE code assumes no gamma-ray attenuation in the computation of results. Some of

FIG. 18. Percent Change in Detector Counting Efficiency as a Function of Sample Thickness for Two Ge(Li) Detectors

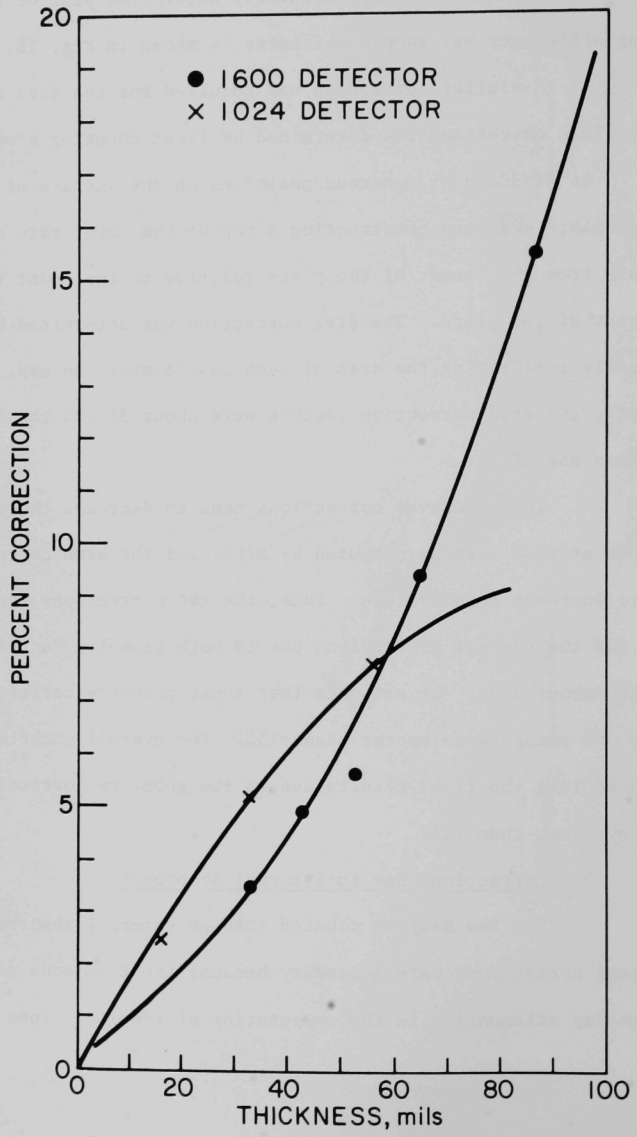

the samples were counted through 35-mil lead, others through 52-mil cadmium; however, most of the samples were counted without any external absorber. The gamma-ray attenuation as a function of energy for each absorber was determined by counting a ^{152}Eu source with and without the absorber. From these measurements, the mass-absorption coefficients for cadmium and lead were determined. Our measurements of the mass-absorption coefficients confirmed that the published values of Berry[12] were appropriate for our samples; thus, the literature values were used for the external absorber corrections. A plot of the gamma-ray attenuation as a function of gamma-ray energy for the lead absorber is shown in Fig. 19.

Corrections to the BILE output for samples counted through an absorber were required for each individual gamma ray. The largest corrections, which occurred for the 293-keV gamma from ^{143}Ce, amounted to about 30% for a lead absorber. We estimate the uncertainty in the external-absorber correction to be about ±5%. This uncertainty results in an uncertainty of about 1.5% in the final activation rates measured for ^{143}Ce, about 1% uncertainty in the ^{103}Ru and ^{131}I values, and less than 0.5% uncertainty for the other fission products.

3. Corrections Due to Self-Absorption

Due to the finite thicknesses of the uranium and plutonium samples, gamma-ray attenuation also occurs by self-abosrption within the samples. The self-absorption is most predominant in the thickest heavy-element samples, and has the greatest effect on the lower-energy

FIG. 19. Gamma-Ray Attenuation (I/I_o) as a Function of Gamma-Ray Energy Due to a 35-mil External Lead Absorber

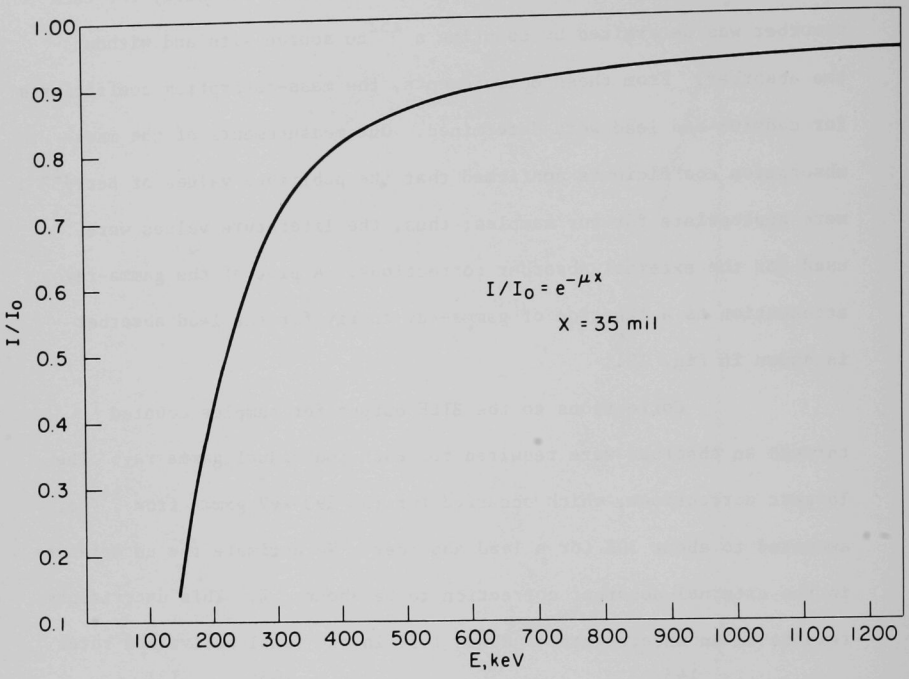

gamma rays. For each nuclide measured, the principal gamma ray was corrected for self-absorption within the sample by means of the approximation:

$$\frac{1 - e^{-ux}}{ux} \qquad (1)$$

where u is the mass-absorption coefficient of the sample in units of cm^{-1} and x is the total thickness of the sample in centimeters. For the gold and nickel samples, this correction was found to be negligible and was not applied. For the uranium and plutonium samples, the mass-absorption coefficients for uranium were used.[13] The literature values were confirmed experimentally by counting a ^{152}Eu standard through various thicknesses of uranium metal foils.

Self-absorption correction factors (I/I_o) as a function of gamma-ray energy are shown in Fig. 20 for several thicknesses of uranium samples. The largest corrections (as great as 45%) were made for the 185-keV gammas from ^{239}Np in the thickest ^{238}U samples. We estimate that these correction factors have been determined with an accuracy of ±10%. The uncertainties in the final absolute reaction rates due to the self-absorption corrections are, in general, about 3 to 4% for ^{239}Np, about 1% for ^{131}I and ^{103}Ru, about 0.5% for ^{95}Zr, ^{97}Zr, and ^{132}Te, and about 0.2% for ^{140}Ba.

4. Correction for Isotopic Impurity

Because the fissionable samples were not 100% isotopically pure, it was necessary to correct for those fission product activities

FIG. 20. Gamma-Ray Self-Absorption (I/I_o) as a Function of Gamma-Ray Energy for 6- , 10- , and 20-mil-thick uranium samples

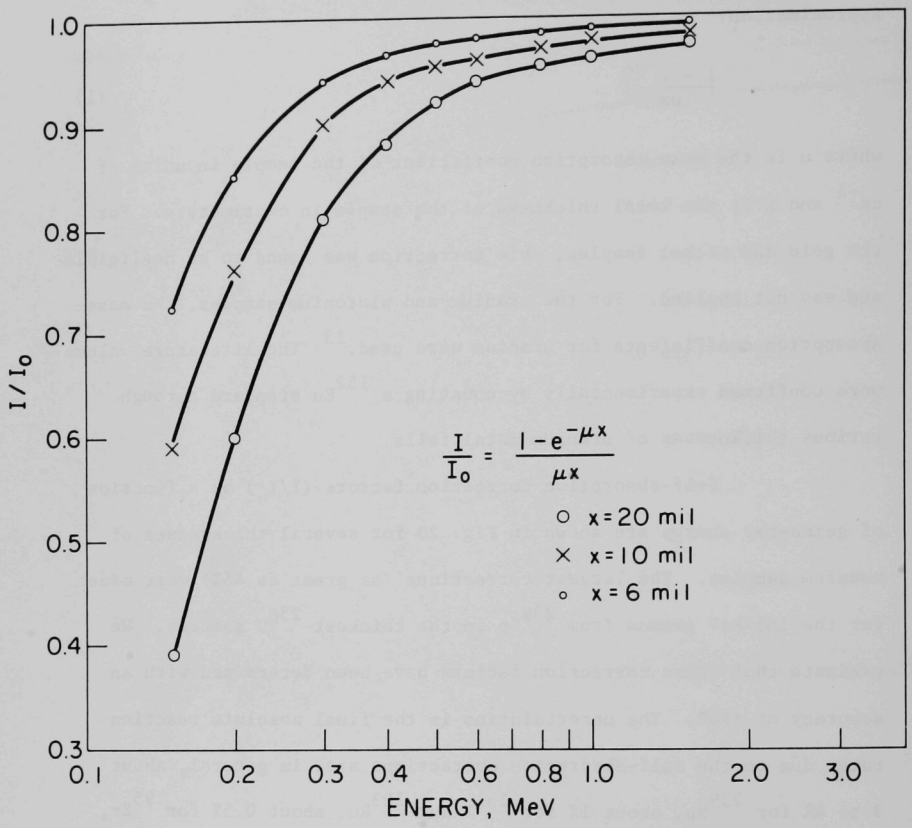

that resulted from isotopes present as impurities. (See Table III.) The correction for ^{238}U fission in the ^{235}U samples was in all cases less than 1%; therefore, this correction was neglected. The correction for ^{235}U fissions in ^{238}U was made as follows:

$$(\sigma\phi)_8 = \frac{[(\sigma\phi)_5 + (\sigma\phi)_8] - 0.002(\sigma\phi)_5}{0.998}$$

where $(\sigma\phi)_8$ is the fission rate of pure ^{238}U in the ^{238}U samples, $[(\sigma\phi)_8 + (\sigma\phi)_5]$ is the fission rate measured including the contributions from ^{238}U and ^{235}U, and $(\sigma\phi)_5$ is the fission rate measured in a pure ^{235}U sample. This correction was about 6% for the ^{238}U interface samples and about 13% for the blanket samples. The uncertainty in the absolute reaction rates due to this correction is estimated to be less than 1%.

5. Effects of Neutron Self-Shielding

The thickest ^{235}U samples irradiated in the fission-yield packets were about 32 mils. In order to ascertain that at this thickness no neutron self-shielding was occurring, the following measurement was performed on the thickest ^{235}U sample irradiated in the softest neutron spectrum of Assembly 60 (a 5BL sample). Approximately 20% of the sample was dissolved in nitric acid; the sample was removed, washed, and weighed; and this treatment was repeated until the entire sample was dissolved. The five resulting solutions each contained about 100 mg of the original sample. These five solutions were counted and the gross activity in each solution was determined. These results indicated

that within an accuracy of 5%, no neutron self-shielding had occurred within the sample.

D. Error Analysis

After the appropriate corrections were made to determine the atoms of each reaction product present at the end of the irradiation, it was necessary to ascertain the uncertainty in each result. For the gold and nickel samples which were counted on NaI(Tl) detector, the following procedure was used. Each sample was counted three times and corrected for decay to give A_o (counts/min) at the time of the end of the irradiation. The uncertainty in A_o, namely δA_o, was computed as the standard deviation of the average of the three measurements. Values of A_o were converted to N_o (atoms at time zero) by the following equation:

$$N_o + \delta N_o = \frac{A_o + \delta A_o}{(\lambda + \delta\lambda)(E + \delta E)\ (BR + \delta BR)} \qquad (2)$$

where λ is the decay constant, E is the detector efficiency, BR is the branching ratio, and δ designates the uncertainty in each value. The quantity δE is the largest uncertainty and is estimated to be 8% for gold and 3% for nickel. A propagation of the errors results in a value for δN_o.

The BILE computer analysis of the Ge(Li) counting data from the fissile samples gives a value for the number of atoms at time zero; after making the corrections cited above, this value becomes the

N_o value. The absolute uncertainty in N_o, namely δN_o, was computed from the following equation:

$$\delta N_o = \left\{ \frac{\sum_{i=1}^{n} \left(\frac{N_o^i}{n} - N_o^i \right)^2}{n(n-1)} + (\delta E)^2 + (\delta BR)^2 + (\delta SA)^2 + (\delta Geo)^2 + (\delta Abs)^2 \right\}^{1/2} \quad (3)$$

where N_o^i is the ith count (measurement) of the reaction product N_o, δSA is the uncertainty in the self-absorption correction factor, δGeo is the uncertainty in the geometry correction factor, and δAbs is the uncertainty in the external absorber correction factor. The quantities δE, δSA, and δAbs are each dependent upon the energy of the gamma ray used to determine N_o; therefore, it is impossible to generalize on the magnitudes of each of these quantities. Each uncertainty assignment was evaluated individually for each fission product in each sample. The rationale for assigning errors is the following: The uncertainty due to efficiency, δE, is between 3 and 5% depending upon the gamma energy; δSA was assigned to be 10% of the self-absorption correction factor; δGeo was assigned to be 10% of the geometry correction factor; δAbs was assigned to be 5% of the external absorber correction factor; and δBR was defined by the uncertainty assigned to the values quoted in the literature.

Since one of the main purposes of these experiments was to evaluate heterogeneity effects, the relative uncertainty between samples in the same drawer location is important. This relative uncertainty, ΔN_o, was determined by

$$\Delta N_o = \left\{ \frac{\sum_{i=1}^{n} \left(\frac{\Sigma N_o^i}{n} - N_o^i \right)^2}{n(n-1)} + (\delta SA)^2 \right\}^{1/2} . \qquad (4)$$

IV. RESULTS

From the number of atoms at the end of the irradiation, N_o, and the respective uncertainty in this value, we can compute the reaction rate for each of the samples from the equation

$$(\sigma\phi) = \frac{\lambda N_o}{n(1 - e^{-\lambda t})} . \qquad (5)$$

The quantity $\sigma\phi$ is the reaction rate computed in units of sec^{-1}, λ is the decay constant for the reaction product in units of sec^{-1}, n is the number of target atoms irradiated in the sample, and t is the time of the irradiation (3660 sec). The quantity $\sigma\phi$ is often referred to as the saturated activity. Table X summarizes the results of the reaction-rate measurements for the $^{197}Au(n,\gamma)^{198}Au$, $^{58}Ni(n,p)^{58}Co$, and $^{238}U(n,\gamma)^{239}Np$ reactions measured in the dosimetry foil sets. The correlation between sample number and location within the foil packet is shown in Fig. 10. Both a relative error and an absolute error are quoted for these reaction rates; the absolute error (see Eq. 3) includes all sources of uncertainty whereas the relative error (see Eq. 4), includes only those uncertainties that influence the relative variation between samples within a packet. Thus, in examining the heterogeneity effects within a cross-sectional area of a drawer, the relative errors would apply; however, if one wishes to compare the measured reaction rate with a calculated rate, the absolute errors must be considered.

TABLE X. Absolute Reaction Rates for the $^{197}Au(n,\gamma)^{198}Au$, $^{58}Ni(n,p)^{58}Co$, and $^{238}U(n,\gamma)^{239}Np$ Reactions Measured in Dosimetry Foils

		$^{197}Au(n,\gamma)^{198}Au$			$^{58}Ni(n,p)^{58}Co$			$^{238}U(n,\gamma)^{239}Np$		
		Reaction Rate [10^{-16} atoms/(atom)(sec)]	Relative Error (%)	Absolute Error (%)	Reaction Rate [10^{-16} atoms/(atom)(sec)]	Relative Error (%)	Absolute Error (%)	Reaction Rate [10^{-16} atoms/(atom)(sec)]	Relative Error (%)	Absolute Error (%)
Blanket	1	32.2	1.6	8.2	0.470	0.7	5.9	16.1	3.8	7.7
	2	35.4	2.1	8.3	0.561	0.7	5.9	18.8	4.8	8.2
	3	37.9	0.6	8.1	0.670	0.5	5.9	21.7	4.2	7.9
	4	39.6	0.6	8.1	0.868	1.2	6.0	21.2	4.4	8.0
Inter-	1	54.1	0.6	8.2	3.42	0.9	5.9	29.3	2.2	7.0
face	2	50.6	1.2	8.1	3.60	1.0	5.9	28.3	2.7	7.2
	3	50.7	0.7	8.1	4.05	0.5	5.9	30.5	4.4	8.0
	4	53.1	0.6	8.1	4.27	0.4	5.8	32.6	3.8	7.6
	5	54.0	0.7	8.1	4.81	0.2	5.8	33.6	4.1	7.8
	6	53.7	0.2	8.1	5.32	0.4	5.8	33.3	2.6	7.1
	7	54.3	0.7	8.1	5.55	0.5	5.9	32.4	2.8	7.2
	8	55.2	0.5	8.1	5.18	0.3	5.8	35.9	5.1	8.3
Core	1	74.5	1.0	8.1	8.31	0.2	5.8	46.2	4.2	7.2
	2	76.0	0.8	8.1	8.40	0.1	5.8	46.0	1.5	6.1
	3	73.0	0.3	8.1	8.74	0.2	5.8	47.5	2.1	6.3
	4	75.1	0.4	8.1	8.48	0.1	5.8	49.8	7.2	9.3
	5	75.4	0.2	8.1	8.73	0.4	5.8	44.7	7.3	9.4
	6	74.5	1.1	8.1	9.10	0.9	5.9	47.6	2.4	6.4
	7	74.2	0.5	8.1	9.27	0.7	5.9	46.4	2.0	6.3
	8	75.3	0.6	8.1	8.60	0.6	5.9	45.9	3.7	7.0
	11	73.2	0.4	8.1	8.47	1.4	6.0	47.0	2.7	6.5
	12	75.3	0.3	8.1	8.60	0.5	5.9	45.3	3.6	6.9
	13	75.8	0.2	8.1	8.97	0.9	5.9	48.8	6.5	8.8
	14	76.1	0.3	8.1	8.75	1.6	6.0	47.6	2.4	6.4
	15	76.4	1.2	8.2	8.92	0.3	5.8	47.9	3.2	6.7
	16	75.7	0.4	8.1	9.39	0.6	5.9	49.3	5.8	8.3
	17	76.7	0.2	8.1	9.54	0.5	5.9	48.8	5.7	8.2
	18	76.5	0.2	8.1	8.81	0.5	5.9	49.5	4.8	7.6
	21	72.2	1.0	8.1	8.58	0.8	5.9	46.9	1.8	6.2
	22	75.6	0.4	8.1	8.62	0.7	5.9	47.6	4.7	7.6
	23	73.7	4.4	9.2	8.97	0.1	5.8	47.5	2.3	6.3
	24	77.1	0.3	8.1	8.66	0.2	5.8	46.4	2.2	6.3
	25	77.3	0.1	8.1	8.92	0.8	5.9	49.9	3.3	6.8
	26	74.5	0.7	8.1	9.37	0.4	5.8	47.2	1.8	6.2
	27	78.1	0.5	8.1	9.53	0.4	5.8	49.0	1.7	6.2
	28	77.9	0.5	8.1	8.85	0.6	5.9	49.5	1.5	6.1

Tables XI and XII summarize the production rates of seven individual fission products measured in the dosimetry-foil (D) sets for ^{235}U and ^{238}U, respectively. The errors quoted in these two tables are for the total or absolute uncertainty assigned to each individual measurement. Table XIII summarizes the production rates of five individual fission products measured in the fission-yield (Y) foil sets for ^{235}U, ^{238}U, and ^{239}Pu. The values in Table XIII are reported on the basis of the total amount of fissile material in each packet; these values were obtained by summing the measurements for each nuclide from the six or seven individual pieces in each packet. The relative errors were determined by a propagation of error analysis, which included uncertainties resulting from counting statistics and corrections for self absorption. The absolute errors include all known sources of uncertainty. For the purposes of determining relative fission-yield ratios or changes in fission yield as a function of neutron spectrum, i.e., position, the relative errors apply; the absolute errors are appropriate for absolute fission-yields determinations.

An individual fission-product reaction rate can be related to the fission rate by

$$(\sigma\phi) = (\sigma_f\phi)(FY) \qquad (6)$$

where $\sigma\phi$ is the number of atoms of a given fission product produced per atom of fissile material per second, FY is the fission yield of the fission product, and $\sigma_f\phi$ is the fission rate or the number of

TABLE XI. Production Rates of Fission Products Measured in ^{235}U Dosimetry Foils

		Fission Product [10^{-15} atoms/(atom ^{235}U)(sec)]													
		^{95}Zr		^{97}Zr		^{103}Ru		^{131}I		^{132}Te		^{140}Ba		^{143}Ce	
Sample		Rate	% Error	Rate	% Error	Rate	% Error	Rate	% Error	Rate	% Error	Rate	% Error	Rate	% Error
Blanket	1	0.997	4.6	0.825	10.8	0.409	7.0	0.428	4.5	0.645	6.1	0.781	3.8	0.577	6.2
	2	1.02	4.5	0.876	3.8	0.454	6.9	0.491	5.9	0.704	6.4	0.850	3.7	0.654	5.9
	3	1.04	7.7	0.953	3.7	0.446	10.4	0.468	6.4	0.735	11.3	0.850	4.6	0.697	10.3
	4	1.18	4.2	1.04	4.0	0.550	7.7	0.578	5.5	0.831	6.5	0.973	4.3	0.738	8.2
Interface	1	1.80	4.7	1.57	7.6	0.809	7.5	0.830	5.6	1.30	8.3	1.39	4.7	1.27	6.0
	2	1.84	4.8	1.63	5.1	0.821	16.8	0.851	5.6	1.32	6.8	1.48	4.7	1.29	5.3
	3	1.96	4.5	1.69	3.7	0.886	6.8	0.909	5.7	1.37	8.6	1.61	4.0	1.21	11.7
	4	1.97	4.0	1.79	3.7	0.880	9.8	0.909	9.2	1.49	9.4	1.56	5.4	1.24	9.2
	5	2.07	4.4	1.78	3.7	0.954	5.8	0.978	7.1	1.37	7.0	1.67	4.1	1.14	6.3
	6	2.03	4.5	-	-	0.920	9.1	0.964	7.3	1.50	7.3	1.64	4.9	1.29	4.8
	7	2.16	4.7	1.97	6.5	0.992	6.4	1.02	5.6	1.55	6.6	1.75	3.9	1.42	7.2
	8	2.21	4.1	2.00	4.6	1.00	6.7	1.06	8.4	1.55	7.6	1.81	5.3	1.40	5.8
Core	1	2.71	5.9	2.80	4.0	1.26	11.6	1.49	3.9	2.02	7.3	2.59	5.0	2.27	6.3
	2	2.90	5.6	2.78	4.0	1.36	6.2	1.42	7.1	1.99	6.6	2.57	7.6	2.33	7.9
	3	2.94	5.7	2.70	4.5	1.49	4.9	1.49	17.2	2.13	10.0	2.62	7.1	2.38	6.7
	4	2.88	5.6	2.70	6.5	1.36	4.3	1.47	5.1	2.00	7.2	2.62	4.7	2.31	6.5
	5	2.90	6.1	2.76	3.6	1.43	3.6	1.48	7.8	1.96	10.1	2.60	6.6	2.34	4.7
	6	3.10	6.1	2.81	3.9	1.42	11.0	1.52	5.3	2.08	6.7	2.54	6.6	2.38	5.2
	7	3.08	6.3	2.89	4.4	1.47	4.1	1.43	4.8	2.15	7.2	2.73	7.9	2.37	19.2
	8	3.10	6.2	2.88	8.6	1.47	8.3	1.53	5.8	2.10	10.6	2.79	7.0	2.39	4.1
	11	3.04	5.8	2.80	4.5	1.41	6.4	1.53	7.2	2.10	10.1	2.57	4.4	2.43	4.6
	12	2.87	5.5	2.79	4.1	1.36	5.9	1.51	5.8	2.04	6.9	2.43	12.1	2.31	5.0
	13	3.00	6.0	2.80	3.4	1.51	7.5	1.48	5.0	2.08	8.5	2.65	4.6	2.42	3.7
	14	3.00	5.7	2.75	3.3	1.31	7.3	1.51	7.4	1.92	8.3	2.52	5.2	2.31	3.6
	15	2.96	5.8	2.80	3.9	1.45	5.7	1.51	6.5	2.04	10.8	2.63	4.5	2.35	3.7
	16	3.04	6.3	2.86	3.8	1.46	4.4	1.57	5.9	2.06	8.0	2.61	4.4	2.38	5.3
	17	3.03	6.7	2.88	3.7	1.46	6.1	1.52	6.0	2.11	7.4	2.67	4.6	2.38	3.8
	18	3.03	5.9	2.86	3.3	1.45	4.4	1.50	7.0	2.04	9.6	2.67	5.0	2.42	3.5
	21	3.10	5.8	2.74	5.4	1.44	5.1	1.58	4.2	2.05	7.8	2.63	8.0	2.31	12.0
	22	2.96	5.5	2.85	7.5	1.43	6.5	1.45	3.5	2.11	9.4	2.59	4.4	2.29	6.8

TABLE XI (Cont'd)

		Fission Product [10^{-15} atoms/(atom ^{235}U)(sec)]													
		^{95}Zr		^{97}Zr		^{103}Ru		^{131}I		^{132}Te		^{140}Ba		^{143}Ce	
Sample		Rate	% Error	Rate	% Error	Rate	% Error	Rate	% Error	Rate	% Error	Rate	% Error	Rate	% Error
Core	23	3.04	6.0	2.80	3.8	1.46	6.7	1.54	7.9	2.13	6.9	2.51	4.4	2.32	3.6
	24	2.96	5.7	2.79	3.4	1.42	7.5	1.39	5.9	2.06	11.6	2.53	4.9	2.25	6.7
	25	2.93	5.8	2.83	3.5	1.36	8.8	1.51	6.9	2.05	7.2	2.52	4.4	2.28	6.8
	26	3.19	6.3	2.88	5.1	1.48	5.7	1.52	6.9	2.04	7.1	2.75	4.5	2.42	3.6
	27	3.07	6.7	2.80	4.0	1.42	4.8	1.63	5.2	2.12	8.7	2.67	4.4.	2.48	3.4
	28	3.08	5.9	2.92	3.7	1.41	6.4	1.59	4.5	2.19	7.6	2.57	4.5	2.46	4.3

TABLE XII. Production Rates of Fission Products Measured in ^{238}U Dosimetry Foils

		Fission Product [10^{-16} atoms/(atom ^{238}U)(sec)]													
		^{95}Zr		^{97}Zr		^{103}Ru		^{131}I		^{132}Te		^{140}Ba		^{143}Ce	
Sample		Rate	% Error	Rate	% Error	Rate	% Error	Rate	% Error	Rate	% Error	Rate	% Error	Rate	% Error
Blanket	1	-	-	0.116	7.3	0.113	5.4	0.062	9.9	0.113	7.3	0.116	5.4	0.079	6.6
	2	0.152	7.4	0.141	7.4	0.164	7.0	0.077	7.5	0.139	7.4	0.135	6.3	0.095	11.5
	3	0.156	5.3	0.183	6.9	0.189	9.6	0.096	8.4	0.177	6.9	0.186	4.5	0.123	8.1
	4	0.201	7.9	0.221	7.3	0.216	5.6	0.118	6.7	0.204	7.3	0.212	5.0	0.156	10.1
Interface	1	0.676	18.8	0.800	6.8	0.804	12.9	0.433	9.4	0.730	6.8	0.746	5.2	0.536	6.3
	2	0.737	10.7	0.830	7.8	0.840	4.7	0.433	7.5	0.761	7.8	0.756	6.0	0.557	7.9
	3	0.919	8.4	0.99	7.8	1.01	6.3	0.499	6.2	0.923	7.8	0.945	3.8	0.666	7.0
	4	0.904	4.8	1.03	7.4	1.03	12.0	0.534	7.3	0.98	7.4	0.99	4.0	0.730	7.2
	5	1.03	5.7	1.14	7.1	1.23	5.8	0.615	5.9	1.08	7.1	1.10	4.2	0.810	6.3
	6	1.18	10.3	1.21	6.9	1.23	6.1	0.641	7.1	1.12	6.9	1.13	4.7	0.827	6.9
	7	1.10	5.8	1.31	6.5	1.24	5.5	0.677	4.9	1.14	6.5	1.17	4.5	0.843	5.9
	8	1.13	4.3	1.26	6.9	1.23	10.0	0.667	8.5	1.10	6.9	1.20	3.7	0.911	9.5
Core	1	1.77	7.4	1.90	9.2	1.89	7.3	1.05	10.8	1.64	9.2	1.79	8.0	1.16	12.5
	2	1.77	8.4	1.92	6.5	1.90	10.2	1.03	9.8	1.59	6.5	1.85	9.8	1.20	4.9
	3	1.61	7.4	2.03	6.2	1.98	6.9	1.12	10.0	1.75	6.2	2.13	16.5	1.24	4.8
	4	1.83	19.4	1.90	7.5	1.89	5.4	0.96	9.6	1.65	7.5	1.75	5.0	1.22	10.6
	5	1.55	11.3	2.96	6.7	2.09	7.3	1.04	9.0	1.70	6.7	1.74	7.3	1.24	3.7
	6	2.04	11.3	2.05	6.5	2.98	4.1	0.97	20.7	1.66	6.5	1.88	5.5	1.25	4.2
	7	2.14	5.6	2.12	9.3	2.17	7.6	1.06	7.9	1.83	9.3	1.94	8.9	1.30	6.2
	8	1.93	14.2	2.00	9.6	1.99	6.1	1.11	11.8	1.73	9.6	1.89	7.3	1.28	7.5
	11	1.93	8.9	1.88	8.1	1.90	4.6	0.96	11.4	1.66	8.1	1.78	5.4	1.23	5.1
	12	1.60	16.1	1.86	6.7	1.88	6.8	1.00	7.2	1.56	6.7	1.83	5.8	1.23	3.9
	13	2.11	18.1	2.08	8.7	2.10	4.9	1.08	7.9	1.83	8.7	2.07	4.9	1.25	8.0
	14	2.17	9.1	1.95	7.5	1.97	4.5	1.05	7.3	1.68	7.5	1.97	5.7	1.31	10.9
	15	1.83	6.2	1.98	8.9	2.00	6.1	1.04	9.6	1.76	8.9	2.03	4.7	1.28	9.3
	16	1.73	11.4	2.04	8.7	2.06	7.5	1.11	14.4	1.78	8.7	2.08	4.4	1.23	10.3
	17	2.13	10.9	2.14	8.7	2.14	9.4	1.09	7.7	1.83	8.7	2.22	4.8	1.34	6.1
	18	2.17	15.2	1.95	7.6	2.08	5.4	0.99	10.3	1.75	7.6	2.00	4.6	1.30	6.7
	21	1.88	13.0	1.80	9.2	2.02	11.7	1.06	11.7	1.58	9.2	1.99	5.8	1.16	4.0

TABLE XII (Cont'd)

Sample		Fission Product [10^{-16} atoms/(atom ^{238}U)(sec)]													
		^{95}Zr		^{97}Zr		^{103}Ru		^{131}I		^{132}Te		^{140}Ba		^{143}Ce	
		Rate	% Error	Rate	% Error	Rate	% Error	Rate	% Error	Rate	% Error	Rate	% Error	Rate	% Error
Core	22	1.66	7.8	1.86	6.7	2.05	7.1	1.12	5.0	1.70	6.7	1.88	5.6	1.19	4.4
	23	1.94	12.2	2.00	7.8	2.10	6.9	1.05	9.8	1.78	7.8	1.98	5.2	1.31	5.7
	24	1.91	7.6	1.90	6.3	1.94	4.3	0.97	7.3	1.73	6.3	1.81	7.1	1.25	12.5
	25	1.68	12.6	2.00	6.2	2.02	3.8	1.07	9.1	1.79	6.2	1.89	5.9	1.21	7.6
	26	1.90	11.6	2.05	6.6	2.08	6.3	1.13	9.0	1.74	6.6	2.05	6.0	1.26	5.0
	27	2.04	12.1	2.19	8.3	2.23	5.8	1.18	11.5	1.82	8.3	2.05	5.8	1.24	11.0
	28	1.74	6.8	2.05	7.5	2.02	10.1	1.12	9.5	1.83	7.5	1.88	10.0	1.35	7.8

TABLE XIII. Production Rates of Fission Products Measured in ^{235}U, ^{238}U, and ^{239}Pu Fission-Yield Foils

	^{95}Zr			^{103}Ru			^{131}I			^{132}Te			^{140}Ba		
		% Error			% Error			% Error			% Error			% Error	
ample	Rate	Rel	Abs	Rate	Rel	Abs	Rate	Rel	Abs	Rate	Rel	Abs	Rate	Rel	Abs
CL	26.6	1.53	4.10	13.2	1.24	3.67	13.4	2.04	4.38	18.2	1.47	6.12	24.0	0.56	3.91
IL	16.7	1.06	3.95	8.71	1.24	3.67	8.69	2.04	4.38	12.1	1.47	6.12	15.8	0.56	3.91
BL	9.56	1.30	4.01	4.78	1.70	3.85	4.72	2.24	4.47	6.41	2.64	6.50	8.58	0.74	3.94
CL	1.50	1.88	4.23	1.69	2.28	4.14	0.94	3.97	5.55	1.41	2.50	6.44	1.67	1.03	4.01
IL	0.75	7.89	9.77	0.93	2.26	4.13	0.51	4.00	5.56	0.75	2.89	6.66	0.90	1.45	4.14
CL	23.34	1.53	4.13	30.30	1.54	3.78	19.89	2.14	4.21	22.13	1.76	6.21	23.46	0.67	3.94
9BL	7.55	3.51	5.20	9.24	4.06	5.33	6.07	4.59	5.85	6.52	4.69	7.58	7.09	3.41	5.16

fissions per second per atom of fissile material. Very accurate fission yields for the fission products measured here will be determined when the counting of the mica track recorders is completed. At present, however, neither the ^{235}U nor the ^{238}U yields for the seven measured fission products are well known. Meek and Rider[14] have summarized numerous fission-product yields for both ^{235}U and ^{238}U fission in a thermal spectrum and in a fission spectrum of neutrons. We have used their recommended yields as a guide in estimating a set of fission-product yields that are relatively self-consistent with our measured fission-product activities. These yields are presented in Table XIV.

The absolute fission rate for each of the dosimetry samples was determined by dividing the sum of the seven, individually measured fission-product reaction rates by the sum of the seven self-consistent fission yields (see Table XIV). Although the uncertainties for the fission yields can only be estimated, the sum of the seven yields is thought to be accurate to ±10-15%. The results of the fission-rate measurements of ^{235}U and ^{238}U from the dosimetry foil sets are presented in Table XV. The relative fission rates presented in this table represent the sum of the seven fission-product reaction rates previously given individually in Tables XI and XII. The relative errors were evaluated by propagating the uncertainty in each individual activity to obtain the overall uncertainty for the sum.

Table XVI summarizes the absolute fission-rate measurements determined from the fission-yield (Y) foil sets. The ^{235}U and ^{239}Pu fission rates have been determined from five measured fission-product

TABLE XIV. Summary of Fission-Product-Yield Information for ^{235}U and ^{238}U

Reaction	Fission Product	Inferred[a] Fission Yield (%)	Meek & Rider[b]	
			Thermal (%)	Fission Spectrum (%)
$^{235}U(n,f)$	^{95}Zr	6.7	6.2	6.7
	^{97}Zr	6.3	5.9	6.77
	^{140}Ba	5.9	6.30	5.6
	^{132}Te	4.5	4.33	5.5
	^{143}Ce	5.3	5.91	5.4
	^{131}I	3.3	2.91	3.7
	^{103}Ru	3.3	3.0	3.5
	Total	35.3	34.5	37.2
$^{238}U(n,f)$	^{95}Zr	5.7		5.8
	^{97}Zr	6.1		4.9
	^{140}Ba	6.1		6.0
	^{132}Te	5.3		4.4
	^{143}Ce	4.0		4.3
	^{131}I	3.4		3.2
	^{103}Ru	6.2		5.8
	Total	36.8		34.4

[a]The inferred fission yields are self-consistent with foils irradiated near the core of Assembly 60.

[b]Recommended fission-yield values from M. E. Meek, B. F. Rider, Ref. 14.

TABLE XV. Fission Rates of ^{235}U and ^{238}U Determined from Dosimetry Foils

Sample		$^{235}U[10^{-15}$ atoms/(atom)(sec)]			$^{238}U[10^{-15}$ atoms/(atom)(sec)]		
		Relative Fission Rate	Relative Error (%)	Absolute Fission Rate	Relative Fission Rate	Relative Error (%)	Absolute Fission Rate
Blanket	1	4.10	2.2	11.6	0.073	4.2	0.200
	2	5.05	1.9	14.3	0.090	2.8	0.243
	3	5.19	3.0	14.7	0.110	2.9	0.300
	4	5.89	2.1	16.7	0.132	2.5	0.360
Interface	1	8.97	2.5	25.4	0.475	4.0	1.29
	2	9.23	2.5	26.1	0.490	2.7	1.33
	3	9.64	2.5	27.3	0.596	2.6	1.62
	4	9.84	2.6	27.9	0.620	2.8	1.68
	5	9.96	2.0	28.2	0.702	2.1	1.91
	6	10.1	2.9	28.6	0.735	2.7	2.00
	7	10.9	2.3	30.9	0.744	2.0	2.02
	8	11.0	2.2	31.2	0.746	2.6	2.03
Core	1	15.1	2.3	42.8	1.12	3.2	3.04
	2	15.4	2.5	43.6	1.12	3.2	3.05
	3	15.8	3.0	44.8	1.18	3.7	3.22
	4	15.3	2.3	43.3	1.11	3.9	3.03
	5	15.5	2.4	43.9	1.09	4.8	2.97
	6	15.9	2.4	45.0	1.17	3.1	3.19
	7	16.1	3.6	45.6	1.25	2.7	3.41
	8	16.3	2.9	46.2	1.19	3.5	3.24
	11	15.9	2.3	45.0	1.13	2.6	3.08
	12	15.3	2.7	43.3	1.09	3.2	2.97
	13	15.9	2.1	45.0	1.25	3.7	3.41
	14	15.3	2.2	43.3	1.18	2.7	3.22
	15	15.7	2.3	44.5	1.19	2.6	3.24
	16	16.0	2.1	45.3	1.20	3.1	3.27
	17	16.1	2.1	45.6	1.28	3.0	3.49
	18	16.0	2.2	45.3	1.20	3.2	3.27
	21	15.9	2.9	45.0	1.14	3.6	3.11
	22	15.7	2.6	44.5	1.14	2.4	3.11
	23	15.8	2.1	44.8	1.21	2.9	3.30
	24	15.4	2.5	43.6	1.14	2.6	3.11
	25	15.5	2.3	43.9	1.16	2.8	3.16
	26	16.3	2.2	46.2	1.21	2.8	3.30
	27	16.2	2.2	45.9	1.27	3.1	3.46
	28	16.2	2.1	45.9	1.19	3.1	3.24

TABLE XVI. Absolute Fission Rates of ^{235}U, ^{238}U, and ^{239}Pu Determined from Fission-Yield Foils

$^{235}U[10^{-15}$ atoms/(atom)(sec)]		$^{238}U[10^{-15}$ atoms/(atom)(sec)]		$^{239}Pu[10^{-15}$ atoms/(atom)(sec)]	
Sample	Absolute Fission Rate	Sample	Absolute Fission Rate	Sample	Absolute Fission Rate
5CL-1	41.7	8CL-1	2.73	9CL-1	51.1
2	40.3	2	2.80	2	50.0
3	40.3	3	2.66	3	49.5
4	39.8	4	2.67	4	50.0
5	39.7	5	2.68	5	50.2
6	39.9	6	2.74	6	50.3
Core Average	40.3	Core Average	2.72	7	51.1
5IL-1	28.2	8IL-1	1.61	Core Average	50.3
2	26.6	2	1.57		
3	26.4	3	1.45		
4	25.8	4	1.40		
5	25.4	5	1.34		
6	24.8	6	1.33		
Interface Average	26.2	Interface Average	1.45		
5BL-1	15.6			9BL-1	17.8
2	15.2			2	16.7
3	14.7			3	16.0
4	14.0			4	15.1
5	13.8			5	14.6
6	13.2			6	14.0
Blanket Average	14.4			7	13.7
				Blanket Average	15.4

rates: ^{95}Zr, ^{103}Ru, ^{131}I, ^{132}Te, and ^{140}Ba. The ^{238}U fission rates were determined from four fission products: ^{103}Ru, ^{131}I, ^{132}Te, and ^{140}Ba. The fission yields used for ^{235}U and ^{238}U were those given in Table XIV; for ^{239}Pu, the same yields as for ^{235}U were used. No errors are quoted in Table XVI because the individual samples were not all counted often enough to give a statistically significant relative error, and the absolute errors are dominated by the uncertainties in the fission yields. The absolute errors are estimated to be about ±15%.

Maddison[8] has reported the results of his measurements from the A foil sets and it is of interest to compare his results with those reported here. His results were reported in units of $(\text{gram-hrs})^{-1}$; therefore, to make a valid comparison, it was necessary to convert his units into units of $(\text{sec})^{-1}$. In addition, his fission-rate values were determined by measuring the fission product, ^{97}Zr, and applying a fission-yield value of 5.77% for ^{235}U and a value of 5.99% for ^{238}U. To provide a consistent comparison, we have converted his results to reflect the fission rates based upon the ^{97}Zr fission yields given in Table XIV.

In Fig. 21 we have plotted the results obtained from the D, Y, and A foil packets irradiated in the core position of Assembly 60. The solid lines indicate the D results, the dashed lines designate the data from the Y packets, and the circles indicate Maddison's data from the A packets. The ordinate of Fig. 21 is the magnitude of

FIG. 21. Comparison of Absolute Reaction Rates in the D, Y, and A Foil Packets Irradiated in the Core Positions

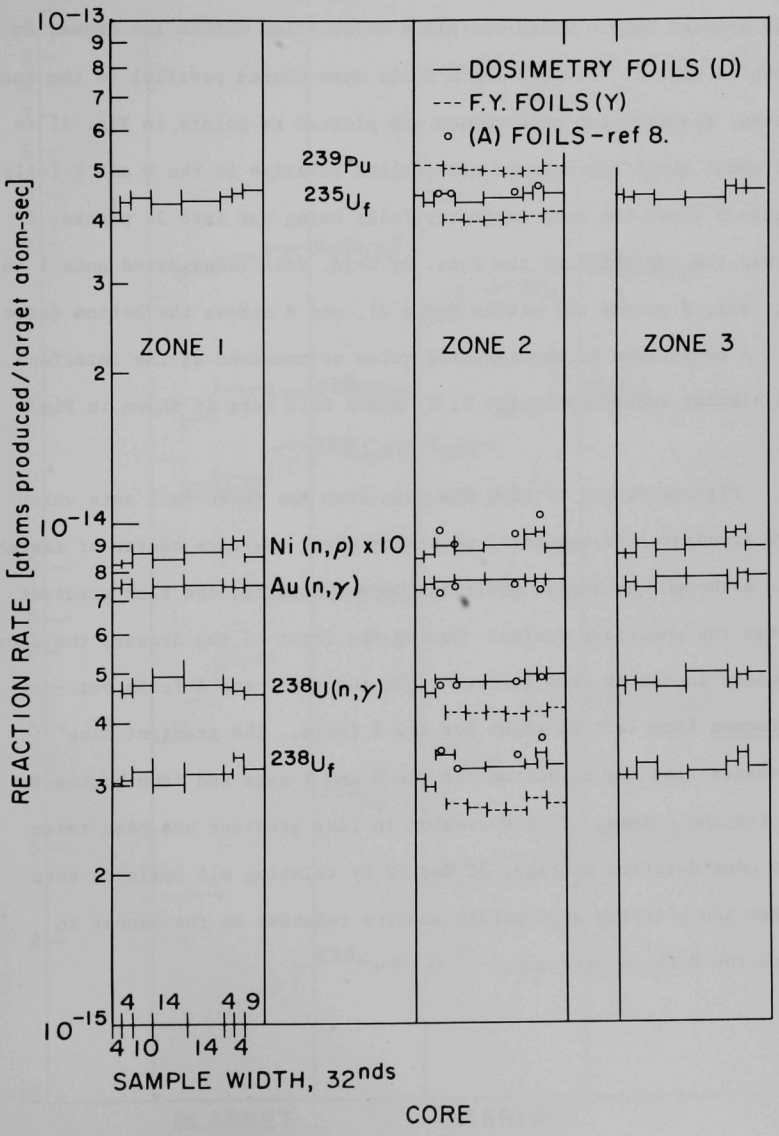

the reaction rate which is represented by solid and dashed lines. The abscissa, which is the length of the solid and dashed lines, corresponds to the approximate width of each sample in 1/32 of an inch. The relationship between sample width and plate orientation within the drawer is shown in Fig. 2. Because the A foils were placed parallel to the fuel plates, the reaction rate values are plotted as points in Fig. 21 to represent their approximate orientation relative to the D and Y foils. Figure 9 shows the core dosimetry foils being cut into 24 pieces, 8 across the top third of the 2-in. by 2-in. foil (designated zone 1 in Fig. 21), 8 across the middle (zone 2), and 8 across the bottom (zone 3). A comparison of the reaction rates as measured at the interface and blanket locations in the D, Y, and A foil sets is shown in Fig. 22.

Figures 21 and 22 show the data from the three foil sets which were irradiated in symmetric positions about the core center of Assembly 60. Although the sample positions were symmetric, the flux gradient across the positions varied. Facing the front of the drawer, the flux gradient increases from left to right for the D and A foils but decreases from left to right for the Y foils. The gradient also increases from top to bottom for the D and Y sets and from bottom to top for the A sets. This variation in flux gradient has been taken into consideration in Figs. 21 and 22 by relating all foils to core center and plotting appropriate samples relative to the manner in which the D foils were cut.

FIG. 22. Comparison of Absolute Reaction Rates in the D, Y, and A Foil Packets Irradiated in the Interface and Blanket Positions

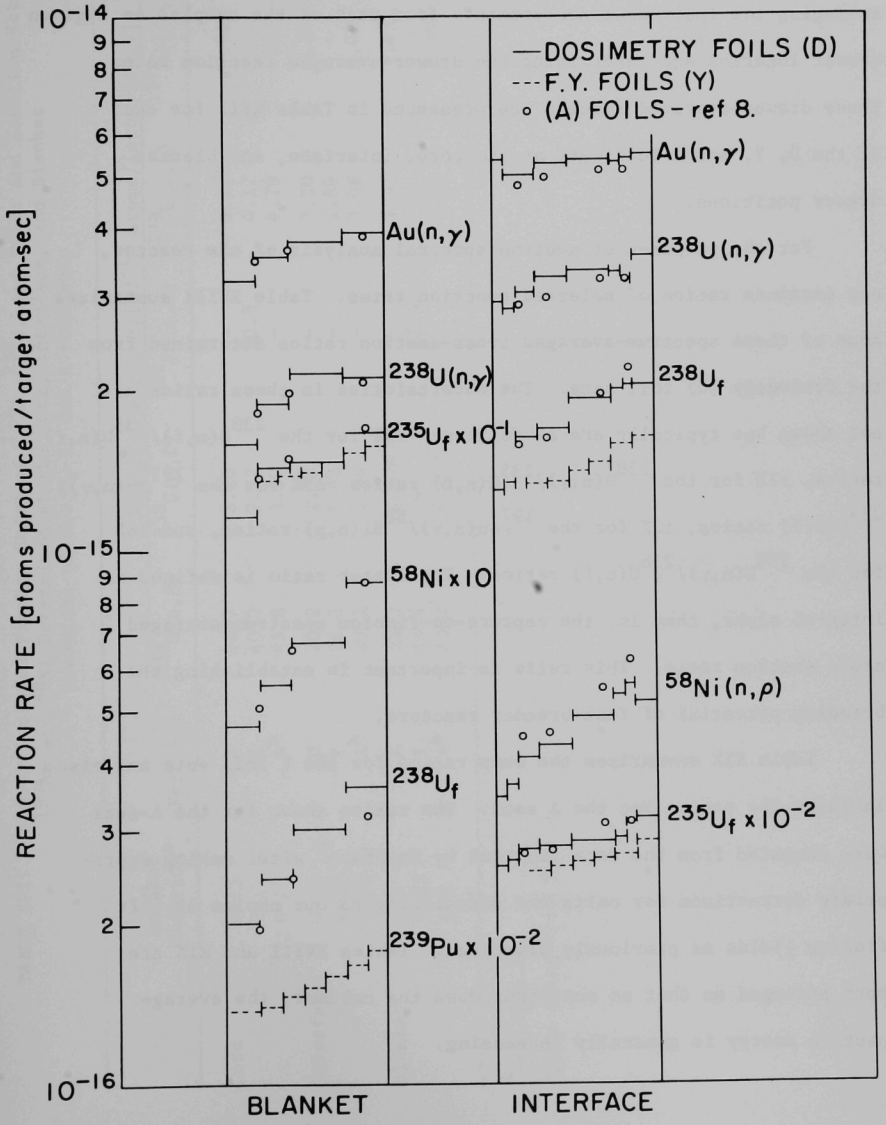

The comparisons of the data from the D, Y, and A foil sets, as shown in Figs. 21 and 22, emphasize the detailed heterogeneity effects within a given drawer location. Another comparison can be made by averaging the individual measurements from each of the samples as a given drawer location and determining the drawer-averaged reaction rates. These drawer-averaged results are presented in Table XVII for each of the D, Y, and A foil sets at the core, interface, and blanket drawer positions.

For the purposes of neutron spectral analysis of the reactor, one examines ratios of selected reaction rates. Table XVIII summarizes some of these spectrum-averaged cross-section ratios determined from the dosimetry (D) foil sets. The uncertainties in these ratios are not shown but typically are as follows: ±5% for the $^{238}U(n,f)/^{235}U(n,f)$ ratios, ±7% for the $^{238}U(n,\gamma)/^{235}U(n,f)$ ratios, ±3% for the $^{197}Au(n,\gamma)/^{235}U(n,f)$ ratios, ±2% for the $^{197}Au(n,\gamma)/^{58}Ni(n,p)$ ratios, and ±8% for the $^{238}U(n,\gamma)/^{238}U(n,f)$ ratios. The latter ratio is defined as integral alpha, that is, the capture-to-fission spectrum-averaged cross section ratio. This ratio is important in establishing the breeding potential of fast-breeder reactors.

Table XIX summarizes the same ratios for the Y foil sets and also includes the ratios for the A sets. The ratios shown for the A sets were computed from the data reported by Maddison[8] after making appropriate corrections for units and normalizing to our choice of ^{97}Zr fission yields as previously discussed. Tables XVIII and XIX are both arranged so that as one reads down the columns, the average neutron energy is generally increasing.

TABLE XVII. Drawer-Averaged Fission Rates of ^{235}U, ^{238}U, and ^{239}Pu and Reaction Rates of ^{197}Au and ^{58}Ni Determined at the Core, Interface, and Blanket Locations of the D, Y, and A Foil Sets

	Reactor Position[a]	Foil Set	Reaction Rate, $\sigma\phi$[10^{-15} atoms/(atom)(sec)]					
			$^{235}U(n,f)$	$^{238}U(n,f)$	$^{239}Pu(n,f)$	$^{238}U(n,\gamma)$	$^{197}Au(n,\gamma)$	$^{58}Ni(n,p)$
Core	O-15	D	44.7	3.20	-	4.77	7.54	0.886
	O-17	Y	40.3	2.72	50.3	4.17	-	-
	Q-15	A[b]	45.8	3.53	-	4.79	7.37	0.959
Interface	O-11	D	28.2	1.74	-	3.20	5.32	0.453
	O-21	Y	26.2	1.45	-	2.89	-	-
	Q-11	A[b]	29.1	1.88	-	3.08	5.08	0.517
Blanket	O-9	D	14.3	0.276	-	1.95	3.63	0.064
	O-23	Y	14.4	-	15.4	-	-	-
	Q-9	A[b]	15.2	0.255	-	1.96	3.69	0.068

[a] See Fig. 1.

[b] Data taken from Ref. 8.

TABLE XVIII. Spectrum-Averaged Cross-Section Ratios Measured in the Dosimetry Foil Sets

Dosimetry Sample		Cross-Section Ratio $\frac{^{238}U(n,f)}{^{235}U(n,f)}$	$\frac{^{238}U(n,\gamma)}{^{235}U(n,f)}$	$\frac{^{197}Au(n,\gamma)}{^{235}U(n,f)}$	$\frac{^{197}Au(n,\gamma)}{^{58}Ni(n,p)}$	$\frac{^{238}U(n,\gamma)}{^{238}U(n,f)}$
Blanket	1	0.0172	0.139	0.278	68.6	8.06
	2	0.0170	0.131	0.248	63.1	7.74
	3	0.0204	0.148	0.258	56.6	7.23
	4	0.0216	0.127	0.237	45.7	5.89
Interface	1	0.0508	0.115	0.213	15.7	2.27
	2	0.0510	0.108	0.194	14.0	2.13
	3	0.0593	0.112	0.186	12.5	1.88
	4	0.0602	0.117	0.190	12.5	1.95
	5	0.0677	0.119	0.191	11.2	1.76
	6	0.0699	0.115	0.187	10.1	1.68
	7	0.0654	0.105	0.176	9.78	1.60
	8	0.0651	0.115	0.177	10.6	1.77
Core	1	0.0710	0.108	0.174	8.96	1.52
	2	0.0700	0.105	0.174	9.05	1.51
	3	0.0729	0.106	0.163	8.35	1.47
	4	0.0700	0.115	0.173	8.87	1.64
	5	0.0677	0.109	0.172	8.63	1.61
	6	0.0709	0.106	0.165	8.19	1.49
	7	0.0748	0.102	0.163	8.01	1.36
	8	0.0701	0.099	0.163	8.76	1.42
	11	0.0684	0.104	0.163	8.64	1.52
	12	0.0686	0.105	0.174	8.76	1.53
	13	0.0758	0.108	0.168	8.46	1.43
	14	0.0744	0.110	0.176	8.72	1.48
	15	0.0728	0.108	0.172	8.57	1.48
	16	0.0722	0.109	0.167	8.07	1.51
	17	0.0765	0.107	0.168	8.04	1.40
	18	0.0722	0.109	0.169	8.68	1.51
	21	0.0691	0.104	0.160	8.42	1.51
	22	0.0699	0.107	0.170	8.77	1.53
	23	0.0737	0.106	0.164	8.21	1.44
	24	0.0713	0.106	0.177	8.90	1.49
	25	0.0720	0.114	0.176	8.66	1.58
	26	0.0714	0.102	0.161	7.96	1.43
	27	0.0754	0.107	0.170	8.19	1.42
	28	0.0706	0.108	0.169	8.80	1.53

TABLE XIX. Spectrum-Averaged Cross Section Ratios Measured in the Fission-Yield Foil Sets and the A Foil Sets

Sample		Fission-Yield Foil Sets				Sample	A Foil Sets					
		$\frac{^{238}U(n,f)}{^{235}U(n,f)}$	$\frac{^{238}U(n,\gamma)}{^{238}U(n,f)}$	$\frac{^{239}Pu(n,f)}{^{235}U(n,f)}$	$\frac{^{238}U(n,\gamma)}{^{235}U(n,f)}$		$\frac{^{238}U(n,f)^a}{^{235}U(n,f)}$	$\frac{^{238}U(n,f)^b}{^{235}U(n,f)}$	$\frac{^{238}U(n,\gamma)^b}{^{235}U(n,f)}$	$\frac{^{197}Au(n,\gamma)^b}{^{235}U(n,f)}$	$\frac{^{197}Au(n,\gamma)^c}{^{58}Ni(n,p)}$	$\frac{^{238}U(n,\gamma)^b}{^{238}U(n,f)}$
Blanket	6	-	-	1.06	-	A-13	0.0133	0.0141	0.133	0.254	69.0	9.38
	5	-	-	1.06	-	12		0.0163	0.132	0.246	56.4	8.05
	4	-	-	1.08	-	11		0.0187	0.124	0.233	44.7	6.62
	3	-	-	1.09	-	A-10	0.0544	0.0581	0.107	0.178	10.9	1.84
	2	-	-	1.10	-	9		0.0588	0.108	0.183	11.2	1.84
	1	-	-	1.14	-	7		0.0637	0.104	0.170	9.53	1.63
Interface	6	0.0536	2.07	-	0.111	6		0.0722	0.105	0.169	8.29	1.46
	5	0.0528	2.12	-	0.112	A- 5	0.0726	0.0770	0.104	0.160	7.56	1.36
	4	0.0543	2.03	-	0.110	4		0.0714	0.104	0.163	8.16	1.46
	3	0.0550	1.99	-	0.109	2		0.0745	0.105	0.163	8.02	1.45
	2	0.0590	1.90	-	0.112	1		0.0793	0.104	0.157	7.10	1.31
	1	0.0572	1.89	-	0.107							
Core	6	0.0687	1.51	1.26	0.104							
	5	0.0674	1.55	1.27	0.105							
	4	0.0672	1.57	1.26	0.105							
	3	0.0662	1.55	1.23	0.102							
	2	0.0694	1.50	1.24	0.104							
	1	0.0655	1.55	1.23	0.101							

[a] Based on fission yields from Ref. 8.

[b] Based on fission yields described in text.

[c] Data taken from Ref. 8.

V. DISCUSSION

An examination of the results presented in Figs. 21 and 22 and Table XVII indicates that the results from the D and A foils agree to within ±5%, which is well within the assigned experimental uncertainties. However, a comparison of the Y-foil results with the D or A results shows that the ^{235}U fission rates and the $^{238}U(n,\gamma)$ reaction rates are 10% lower than the D or A, and the ^{238}U fission rates are about 15% lower in the core positions. This difference is considered to be outside the experimental uncertainties of the relative values. A possible explanation for this difference was at first considered to be neutron self-shielding, since the Y foils were about twice as thick as the D foils. However, the experimental test for neutron self-shielding on one of the Y foils indicated that the fission rates were affected by less than 5% due to self-shielding in the thickest samples.

The more probable explanation involves two factors. Firstly, the Y foil packets were contained in 125-mil-thick aluminum holders, whereas the D packets were only 30-50 mils thick. The thicker Y packets resulted in a wider separation of the fuel plates at the packet positions and the relatively large amount of aluminum would contribute some neutron down-scatter. This could result in a lower absolute flux and a slightly softer spectrum for the Y foils than for the D foils. Secondly, the assumption of flux and spectral symmetry about the core center may not be valid. Source tubes located on the right side of Half 1 of Assembly 60 (the side in which the Y foils were located) could contribute to both a slight flux reduction and a spectral softening for the Y foils

relative to the D foils. The observation that all reaction rates measured in the Y foils are lower than comparable rates in the D foils, with the $^{238}U(n,f)$ rate showing the greatest difference, indicates both a flux and a spectral depression were experienced by the Y foils; this observation is consistent with the explanation given above.

The reaction rate ratios presented in Tables XVIII and XIX can be used as spectral indices to reflect the changes in the neutron spectra as a function of position within the reactor. Of the spectrum-averaged cross-section ratios presented, the $^{197}Au(n,\gamma)/^{58}Ni(n,p)$ ratio is clearly the most sensitive index to spectral change. The ^{197}Au reaction occurs principally with neutrons having energies below 1 MeV, and the ^{58}Ni reaction occurs only with neutrons having energies above 1 MeV. The $^{197}Au/^{58}Ni$ reaction ratio decreases nearly an order of magnitude between the softer blanket position and the hardest core position. Similarly, this index varies about 15% in going across a horizontal cross section of a reactor drawer in the core position, and thus gives a sensitive indication of the heterogeneity within a drawer due to the plate configuration from which the reactor is constructed. The more commonly used spectral index for reactors, $^{238}U(n,f)/^{235}U(n,f)$ is considerably less sensitive to heterogeneities and is measured less accurately.

The primary objective of these activation-rate measurements was to obtain data for characterizing the irradiation environment of EBR-II. In early 1971, similar foil-activation-rate measurements will be

conducted throughout the core and core-blanket interface regions of EBR-II during both low- and full-power operations. Comparisons of the mockup data and the EBR-II data will define the degree to which Assembly 60 simulates EBR-II and, most importantly, will establish the applicability of the proton-recoil measurements, fission-rate transverses, gamma-heating experiments, and all reactor-physics calculations in Assembly 60 to various loadings of EBR-II. The results of some of these measurements have been reported.[15,16]

The more immediate objective, however, is to provide data from which fast-neutron fission yields may be determined and to provide experimental data with which reactor-physics calculations may be compared. These reported results provide bench-mark information on a well-defined reactor configuration and can be used to evaluate the status of neutronic calculational capability and cross section data required for neutronic calculations.

In summary, we have described the foil-activation-rate measurements made in Assembly 60 and have attempted to present the results in a usable fashion. Reports similar to this one on the activation rate measurements in Assemblies 61, 62, and 63 of the EBR-II mockup program conducted in ZPR-III are now being prepared. More thorough discussions of how these data will be utilized for characterizing a reactor environment, and for establishing fast-neutron fission yields will be the subjects of subsequent reports.

ACKNOWLEDGMENTS

We specifically acknowledge the help, discussions, and suggestions of D. Meneghetti, W. Loewenstein, and W. P. Keeney which resulted in the successful completion of this experiment. R. O. Vosburgh, J. M. Gasidlo, and the operating staff of ZPR-3 were particularly valuable in assisting with loading, irradiating, and removing the samples from the reactor. H. J. Howard and E. D. Duke of SPM were instrumental in facilitating receipt of the samples from Idaho in record-breaking time. Additional recognition is warranted to several individuals for their effort in various phases of the experiment: J. Williams, for her assistance in the preparation, cutting, and mounting of the samples for analysis; R. J. Armani for preparation of the mica track recorders and his expertise in their use as absolute fission rate monitors; M. T. Laug and G. E. Staahl for their uranium mass-spectrometric isotope-dilution analyses; and R. L. Malewicki and C. L. Blogg for their assistance in counting the samples. M. S. Foster provided essential support to the data processing for computer analysis, and G. M. Kesser's editorial assistance enabled this report to be comprehensible.

REFERENCES

1. N. D. Dudey and R. R. Heinrich, Flux Characterization and Neutron-cross-section Studies in EBR-II, ANL-7629 (May 1970).

2. W. N. McElroy, J. L. Jackson, J. A. Ulseth, and R. L. Simons, EBR-II Dosimetry Test Data Analysis (Reactor Runs 31E and 31F), BNWL-1402 (June 1970).

3. L. S. Kellogg and W. H. Zimmer, EBR-II Dosimetry Test Reaction Rate Measurements (Reactor Runs 31E and 31F), BNWL-1403 (June 1970).

4. F. S. Kirn, EBR-II as a Fast Reactor Irradiation Facility, Nucl. News 13, 62-68 (1970).

5. A. Withop, B. A. Hutchins, and G. C. Martin, Analytical Procedures and Applications of Fluence Determinations from EBR-II Flux Wires, GEAP-5744 (1969).

6. W. P. Keeney and D. Meneghetti, pp. 37-39 in Reactor Development Program Progress Report, February 1970, ANL-7669 (Mar 30, 1970)

7. L. Beller and D. Maddison, pp. 42-48 in Reactor Development Program Progress Report, April-May 1970, ANL-7688 (July 14, 1970).

8. D. W. Maddison, pp. 27-34 in Reactor Development Program Progress Report, August 1970, ANL-7737 (Sept 29, 1970)

9. R. J. Armani, R. Gold, R. P. Larsen, and J. H. Roberts, Trans. Am. Nucl. Soc. 13(1), 90 (1970)

10. R. Gold, R. J. Armani, and J. H. Roberts, Absolute Fission Rate Measurements with Solid State Track Recorders, Nucl. Sci. Eng. 34, 13-22 (1968).

11. R. Gunnink, H. B. Levy, and J. B. Niday, Identification and Determination of Gamma Emitters by Computer Analysis of Ge(Li) Spectra, UCID-15140 (May 16, 1967).

12. Peter F. Berry, Gamma-Ray Attenuation Coefficients, Nucleonics 19(6), 62 (June 1961).

13. Handbook of Chemistry and Physics, 49th edition, pp. E-134, E-135, Chemical Rubber Publishing Co., Cleveland, Ohio (1969).

14. M. E. Meek and B. F. Rider, Summary of Fission Product Yields for ^{235}U, ^{238}U, ^{239}Pu, and ^{241}Pu at Thermal, Fission Spectrum, and 14-MeV Neutron Energies, APED-5398 (Mar 1, 1968).

15. W. P. Keeney, R. O. Vosburgh, and D. Meneghetti, pp. 16-24 in Reactor Development Program Progress Report, March 1970, ANL-7679 (Apr 27, 1970).

16. G. G. Simons, pp. 35-42 in Reactor Development Program Progress Report, April-May 1970, ANL-7688 (July 14, 1970).

17. Thomas H. Handley and J. H. Cooper, Anal. Chem. 41, 381 (1969).

APPENDIX A

Preparation of Track Recorders

I. Preparation of Track Recorders

The measurement most crucial to the success of measuring absolute fission yields is the ability to accurately establish the absolute fission rate at a specific location within the reactor. This measurement was accomplished by the use of mica, solid-state track recorders (SSTR)[10] in contact with very thin fission sources. The SSTRs were mica strips 11/32 in. wide, 1 5/16 in. long, and 0.0127 cm thick. The fission sources were circular spots, 5 mm in diameter, deposited on platinum strips having the same dimensions as the mica.

Prior to the irradiation, the mica SSTRs were pre-etched in 49% HF for 6 hr. This is done to develop very large "fossil" fission-fragment tracks that have been produced by the spontaneous fission of the natural uranium impurities contained in the mica. The SSTRs for use in this experiment were selected on the basis of clarity and low number of "fossil" tracks. After the irradiation and exposure to the fission sources, the SSTRs were again etched in 49% HF, but this time for 90 min. The new fission tracks formed during the irradiation are much smaller and easily distinguishable from the "fossil" tracks. Counting of the tracks produced in this experiment has not been completed; the results will be included in a future report discussing the determination of absolute fission yields.

II. Deposition of Nanogram Amounts of Fissile Material on Platinum Strips

The method used to deposit the submicrogram amounts of fissile material on the platinum strips was a modification of the method of

Handley and Cooper[17] for electrodeposition from dimethyl sulfoxide (DMSO). The apparatus used for the electrodeposition is shown in Figure A-1. The apparatus consisted of a 2 in. by 3 in. by 3/8 in. copper block support, a pyrex glass chimney, a platinum electrode, and a d.c. power supply. The glass chimney was made by sealing off and flattening one end of a 1.2 cm internal diameter pyrex tube. A 1.9 cm diameter shoulder was made near the flattened end to enable the chimney to be held by a ball and socket clamp. A 5 mm hole was made in the center of the flattened end and the flattened end was ground to enable a seal to be made between it and the platinum plate upon which it would rest. The platinum electrode was made by looping one end of a 6 in. piece of 0.04 in. diameter wire into a 1 cm diameter circle and spot welding platinum gauze to the circular portion of the platinum wire. The circle was then bend so that its plane was perpendicular to the straight piece of platinum wire.

The electrodeposition procedure used is as follows:

Electrodeposition Procedure

1) Pipet into a 10-ml beaker an appropriate aliquot of a solution of fissile material in dilute ($\sim$3N) HNO_3.
2) Evaporate the solution to dryness.
3) Dissolve in 3 ml dimethylsulfoxide (DMSO) by heating in a hot water bath for 30 min.
4) Transfer the solution to a 10-ml volumetric flask and make up to volume with DMSO.

FIG. A-1. Schematic Diagram of Electroplating Apparatus

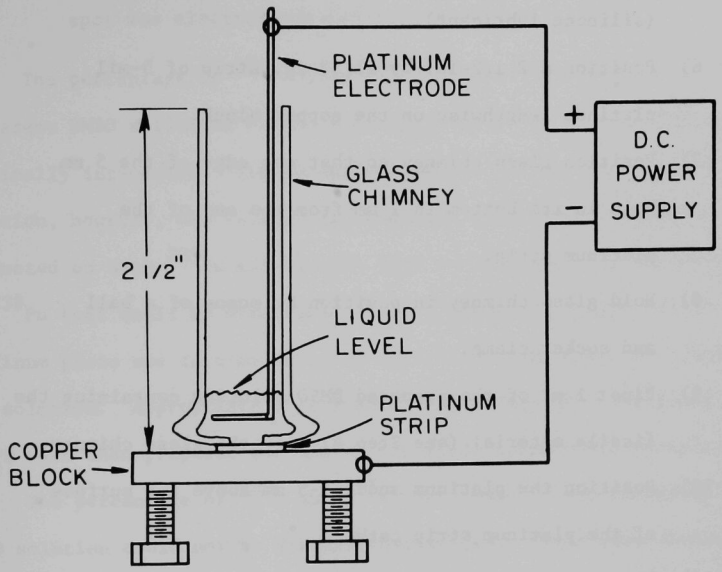

5) Grease the ground-glass surface on the bottom end of the glass chimney with Dow Corning High Vacuum Grease (silicone lubricant).

6) Position a 2 1/2-in. by 11/32-in. strip of 5-mil platinum lengthwise on the copper block.

7) Position glass chimney so that one edge of the 5 mm hole in its bottom is 7 mm from the end of the platinum strip.

8) Hold glass chimney in position by means of a ball and socket clamp.

9) Pipet 1 ml of the prepared DMSO solution containing the fissile material (see Step 4) into the glass chimney.

10) Position the platinum anode 4-5 mm above the surface of the platinum strip cathode.

11) Electroplate at a current of 4 mA for 5 min using a regulated dc power supply capable of delivering up to 1000 V and 100 mA.

12) Remove platinum anode from chimney.

13) Decant DMSO solution from the chimney.

14) Remove platinum cathode from contact with glass chimney.

15) Wash platinum cathode with chloroform to remove grease and excess DMSO.

16) Electrodeposit three more spots of fissile material on this platinum strip with a distance of 7 mm between each.

17) Fire plate to red heat in Meeker burner.

18) Cut platinum strip at the end nearest where the last spot was electrodeposited to a length of 1 15/16 in.

The percentage of ^{239}Pu that could be electroplated from different DMSO solutions varied from 2 to 30% of the amount that was originally introduced. The percentage deposited from any one DMSO solution, however, was relatively constant. Tests were therefore conducted on each ^{239}Pu solution in DMSO to determine the percentage of ^{239}Pu that could be electroplated (the amount deposited on the platinum plate was determined by 2π alpha counting) from the particular solution. Appropriate dilutions of the tested DMSO solutions of ^{239}Pu were then prepared for use in the electrodeposition procedure.

The percentage of ^{235}U and ^{238}U that could be electroplated from DMSO solution could not be directly determined. Tests were conducted using ^{233}U to determine the percentage of uranium that could be electroplated (the amount of ^{233}U deposited on platinum plate was determined by 2π alpha counting) from DMSO solution. The percentage deposited from several different DMSO solutions was consistently between 50 to 60%. The ^{235}U and ^{238}U solutions in DMSO to be used used for electroplating were prepared taking this into consideration.

The ^{239}Pu used in the preparation of the fission track detectors contained only 8 ppm ^{240}Pu. An alpha pulse-height analysis indicated no significant amount of ^{238}Pu present. The ^{235}U used in the preparation of the fission track detectors had an isotopic purity of 99.986% ^{235}U. The ^{238}U contained only 2 ppm ^{235}U, 2 ppm ^{234}U, and 2 ppm ^{236}U.

APPENDIX B

Determination of the Amounts of Fissile Material in Contact with the Mica Track Recorders

Because the electrodeposition procedure used to electroplate the fissile material onto the platinum backing material was not quantitative, it was necessary to determine the exact amount of fissile material in contact with each mica track recorder. The amount of plutonium on each plate was determined by counting the ^{239}Pu alpha activity in a calibrated 2π gas-proportional alpha counter. The intended procedure for determining the ^{238}U and ^{235}U involved dissolving the electrodeposited uranium off the platinum plates with nitric acid, adding to the solution a known amount of ^{233}U and determining the ^{235}U or ^{238}U content of each plate by mass-spectrometric isotope-dilution techniques. The dissolution procedure was evaluated in tests with a ^{233}U sample that had been prepared in a manner identical to the samples. These tests indicated that the uranium could not be quantitatively removed from the plutonium.

It was therefore necessary to devise a new procedure which would allow us to quantitatively establish the uranium content of each plate. The procedure was to dissolve the entire platinum sample, remove the platinum from the uranium by mercury-cathode electrolysis in order to avoid interferences in the mass spectrometric analysis, and finally establish the number of uranium atoms by the mass spectrometric isotopic dilution technique. This method is described in detail below:

Method for Removing, Separating, and Preparing the Uranium on the Platinum Plates for Mass Analysis

1) Remove the platinum strips from the irradiation assembly.
2) Cut the platinum strips into sections corresponding to the electrodeposited samples.
3) Place a sample in a 125-ml Erlenmeyer flask.
4) Add a known amount of ^{233}U spike which is in dilute HNO_3 solution to the Erlenmeyer flask (Note: the amount of ^{233}U added should be approximately equal to the amount of ^{238}U or ^{235}U present.
5) Dissolve the sample in aqua regia (3:1, $HCl:HNO_3$) by heating on a sand bath.
6) Transfer the solution to a 50-ml beaker.
7) Add 1 ml of conc. H_2SO_4 and take to fumes of H_2SO_4 on a sand bath.
8) After cooling, add 20 ml deionized H_2O to the sample.
9) Heat, if necessary, to dissolve the sample.
10) Transfer the sample to the cell of the Dyna-Cath* to which has been added 35 ml of mercury.
11) Position the anode and the cathode connector.
12) Electrolyze for 1 hr at a current of 5 A.
13) Raise the anode and the cathode connector out of the solution.
14) Drain the solution into a 100-ml beaker.

*A commercially available mercury-cathode electrolysis instrument manufactured by the Eberbach Corporation.

15) Wash the anode, the cathode connector, and the cell with approximately 25 ml deionized water.

16) Drain the wash solution into the 100-ml beaker.

17) Pass the solution through a Whatman #50 filter paper and collect in another 100-ml beaker.

18) Take the solution to dryness.

19) Add 5 ml conc. HNO_3 and take to dryness.

20) Add 5 ml conc. HNO_3 and heat for approximately 5 min.

21) Transfer the solution to a 15 ml beaker.

22) Wash the 100-ml beaker with 5 ml 3$\underline{N}$ HNO_3 and transfer the wash solution to the 15 ml beaker.

23) Take the solution to dryness.

24) Add 2 ml conc. HNO_3 and take to dryness.

25) Add 1 ml 3$\underline{N}$ HNO_3 and heat gently.

26) Transfer the solution with a transfer pipet to a 15-ml centrifuge tube with a screw-on plastic cap.

27) Wash the beaker with two 1-ml portions of 3$\underline{N}$ HNO_3 and transfer these to the centrifuge tube.

28) Carefully take the solution to dryness.

29) Add one drop 3$\underline{N}$ HNO_3 to the 15 ml centrifuge tube.

30) Agitate the tube in a vortex mixer.

31) Submit sample for mass-spectrometric analysis.

APPENDIX C

Description of the BILE Computer Code

The computer code BILE is a modification of a gamma-ray analysis code originally written by R. Gunnink, H. B. Levy, and J. B. Niday[11] at Lawrence Radiation Laboratory at Livermore, California. When obtained, the program was written in an LRL language, FORTRAN-400 for CDC computers. Thus, the code was first rewritten in FORTRAN-IV to be compatible with the Argonne IBM-360 50/75 computer system. Additional programming changes were required to enable the code to accommodate data from our 4096-, 1600-, and 1024-channel analyzers in input form of either a magnetic tape or punched paper tape. A brief description of those aspects of the code which influence accuracy and reliability of the activation-rate measurements will now be presented.

Peaks within the spectrum are located by describing a tangent to the peak and noting where the tangent changes sign. Peak boundaries are determined by noting in both the forward and backward direction where the slope of the peak either levels off or changes sign. If an overlap of two or three peaks occurs, the boundary is determined in the same manner but after the last peak in the cluster. Background is determined by subtracting the area under the defined boundaries from the gross counts under the peak. A statistical uncertainty is then assigned to the net count under the peak.

Peak energies are determined by relating the peak position or channel number to a unique polynomial equation which describes the nonlinearity of the counting system. This polynomial is generated

as part of an auxillary library program which is discussed later. Part of the main program input requires a relationship between energy and channel position which is linearly proportional to this polynomial.

The auxillary library program contains such information as nuclide numbers, half-lives, parent-daughter relationships, accurate gamma-ray energies and branching ratios, efficiency calibrations, and geometry factors. In addition to the primary gamma-ray of a particular nuclide, up to two associative gamma-rays are also listed and these are used primarily for purposes of identification. All decay scheme information is organized and cross-reference indexed so that the main program can expeditiously find its required information without time-consuming searches through numerous arrays. The detector efficiency information is generated in the manner described previously, namely, from absolute gamma-ray standards. To these nuclide efficiencies, a polynomial of up to 6th order is least-square fitted by the auxillary program. Efficiencies ranging in energy from 40 keV to 2.0 MeV are calculated using the best-fit polynomial. These calculated efficiencies are adjusted for the particular counting geometry of the sample and are then used in converting counts per minute to photons per minute.

Peak identification is also accomplished with the aid of the information stored on the library tape. Six criteria must be met before a positive identification can be realized. The first of these is that the computer-determined energy of a given peak must fall within ±3 keV of the library energies. Since several nuclides may have energies

within this criteria, other tests must be made to eliminate unlikely candidates. These are an evaluation of half-life vs decay time and the search for associative gammas. Each associative gamma-ray must also meet an energy test criteria and a relative-intensity test criteria. How well a candidate scores on these tests is determined by multiplying each test score together to obtain a confidence index. The nuclide with the highest confidence index is then identified as being responsible for the peak or peaks in question. The success of this portion of the program depends primarily upon accurate efficiency calibration of the detector and an accurate knowledge of gamma-ray energies and intensities. In Table IX are listed the pertinent decay scheme data for nuclides which are reported here.

The nuclides that have been positively identified are summarized conveniently in a table according to isotope, peak energy, disintegrations per minute (dpm) at count time, dpm at zero time, atoms at zero time, a statistical percent error, and the test confidence index. In addition to this table, which is the most useful, several intermediate tables are also printed including one listing unidentified peaks. Also available in the program is the option for a computer plot of the spectrum.

B